

Synthesis and Characterization of a Series of Structurally and Electronically Diverse Fe(II) Complexes Featuring a Family of Triphenylamido-Amine Ligands

Patrina Paraskevopoulou,^{†,‡} Lin Ai,^{†,§} Qiuwen Wang,[†] Devender Pinnapareddy,[†] Rama Acharyya,[†] Rupam Dinda,[†] Purak Das,[†] Remle Çelenligil-Çetin,^{||} Georgios Floros,[‡] Yiannis Sanakis,[‡] Amitava Choudhury,[†] Nigam P. Rath,[#] and Pericles Stavropoulos^{*,†}

[†]Department of Chemistry, Missouri University of Science and Technology, Rolla, Missouri 65409,

[‡]Department of Inorganic Chemistry, Faculty of Chemistry, University of Athens, Panepistimioupoli

Zographou 15771, Athens, Greece, [§]College of Chemistry, Beijing Normal University, Beijing 100875, China,

^{||}Department of Chemistry, Boston University, Boston, Massachusetts 02215, [‡]Institute of Materials Science, NCSR “Demokritos”, Ag. Paraskevi 15310, Greece, and [#]Department of Chemistry and Biochemistry, University of Missouri—St. Louis, St. Louis, Missouri 63121

Received August 7, 2009

A family of triphenylamido-amine ligands of the general stoichiometry $L^xH_3 = [R-NH-(2-C_6H_4)]_3N$ ($R=4-t\text{-BuPh}$ (L^1H_3), 3,5-*t*-Bu₂Ph (L^2H_3), 3,5-(CF₃)₂Ph (L^3H_3), CO-*t*-Bu (L^4H_3), 3,5-Cl₂Ph (L^5H_3), COPh (L^6H_3), CO-*i*-Pr (L^7H_3), COCF₃ (L^8H_3), and *i*-Pr (L^9H_3)) has been synthesized and characterized, featuring a rigid triphenylamido-amine scaffold and an array of stereoelectronically diverse aryl, acyl, and alkyl substituents (R). These ligands are deprotonated by potassium hydride in THF or DMA and reacted with anhydrous FeCl₂ to afford a series of ferrous complexes, exhibiting stoichiometric variation and structural complexity. The prevalent $[(L^x)\text{Fe(II)}-\text{solv}]^-$ structures ($L^x=L^1, L^2, L^3, L^5$, solv=THF; $L^x=L^8$, solv=DMA; $L^x=L^6, L^8$, solv=MeCN) reveal a distorted trigonal bipyramidal geometry, featuring ligand-derived $[N_{3,\text{amido}}N_{\text{amine}}]$ coordination and solvent attachment trans to the N_{amine} atom. Specifically for $[(L^8)\text{Fe(II)}-\text{DMA}]^-$, a N_{amido} residue is coordinated as the corresponding N_{imino} moiety ($\text{Fe}-\text{N}(\text{Ar})=\text{C}(\text{CF}_3)-\text{O}^-$). In contrast, compounds $[(L^4)\text{Fe(II)}]^-$, $[(L^6)_2\text{Fe(II)}_2]^{2-}$, $[\text{K}(L^7)_2\text{Fe(II)}_2]^{2-}$, and $[\text{K}(L^9)\text{Fe}]_2$ are all solvent-free in their coordination sphere and exhibit four-coordinate geometries of significant diversity. In particular, $[(L^4)\text{Fe(II)}]^-$ demonstrates coordination of one amidato residue via the O-atom end ($\text{Fe}-\text{O}-\text{C}(t\text{-Bu})=\text{N}(\text{Ar})$). Furthermore, $[(L^6)_2\text{Fe(II)}_2]^{2-}$ and $[\text{K}(L^7)_2\text{Fe(II)}_2]^{2-}$ are similar structures exhibiting bridging amidato residues ($\text{Fe}-\text{N}(\text{Ar})-\text{C}(\text{R})=\text{O}-\text{Fe}$) in dimeric structural units. Finally, the structure of $[\text{K}(L^9)\text{Fe}]_2$ is the only example featuring a minimal $[N_{3,\text{amido}}N_{\text{amine}}]$ coordination sphere around each Fe(II) site. All compounds have been characterized by a variety of physicochemical techniques, including Mössbauer spectroscopy and electrochemistry, to reveal electronic attributes that are responsible for a range of Fe(II)/Fe(III) redox potentials exceeding 1.0 V.

Introduction

Recent advances in metal-mediated catalysis and enzymology¹ have provided a plethora of examples in which ligand residues contribute as redox-active partners during turnover. Ligand frameworks, which were in the past considered to solely convey stereoelectronic attributes to metal sites, are now scrutinized with greater frequency as potential participants in

storing and transferring redox equivalents. Typical examples of this trend include ligand scaffolds with nitrogen-rich residues (Chart 1) such as diimines,² bis(imino)pyridines,³ PNP pincer ancillaries,⁴ and even *N*-heterocyclic carbenes.⁵

Although the aforementioned ligands, and those described in the present work, are not biomimetic in nature, it is worth

*To whom correspondence should be addressed. Tel.: (+1) 573-341-7220. Fax: (+1) 573-341-6033. E-mail: pericles@mst.edu.

(1) Stubbe, J.; van der Donk, W. A. *Chem. Rev.* **1998**, *98*, 705–762.

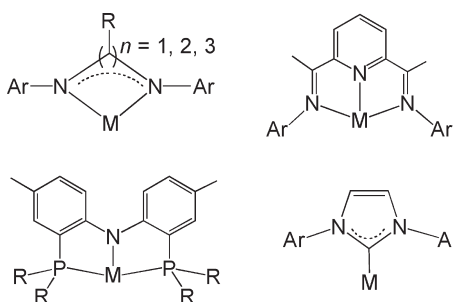
(2) (a) Rose, R. P.; Jones, C.; Schulten, C.; Aldridge, S.; Stasch, A. *Chem.—Eur. J.* **2008**, *14*, 8477–8480. (b) Muresan, N.; Lu, C. C.; Ghosh, M.; Peters, J. C.; Abe, M.; Henling, L. M.; Weyhermüller, T.; Bill, E.; Wieghardt, K. *Inorg. Chem.* **2008**, *47*, 4579–4590. (c) Smith, J. M.; Sadique, A. R.; Cundari, T. R.; Rodgers, K. R.; Lukat-Rodgers, G.; Lachicotte, R. J.; Flaschenreim, C. J.; Vela, J.; Holland, P. L. *J. Am. Chem. Soc.* **2006**, *128*, 756–769. (d) Mindiola, D. J. *Angew. Chem., Int. Ed.* **2009**, *48*, 6198–6200.

(3) (a) Bart, S. C.; Bowman, A. C.; Lobkovsky, E.; Chirik, P. J. *J. Am. Chem. Soc.* **2007**, *129*, 7212–7213. (b) Trovitch, R. J.; Lobkovsky, E.; Bill, E.; Chirik, P. J. *Organometallics* **2008**, *27*, 1470–1478. (c) Trovitch, R. J.; Lobkovsky, E.; Chirik, P. J. *J. Am. Chem. Soc.* **2008**, *130*, 11631–11640.

(4) (a) Ozerov, O. V.; Guo, C.; Papkov, V. A.; Foxman, B. M. *J. Am. Chem. Soc.* **2004**, *126*, 4792–4793. (b) Adhikari, D.; Mossin, S.; Basuli, F.; Huffman, J. C.; Szilagyi, R. K.; Meyer, K.; Mindiola, D. J. *J. Am. Chem. Soc.* **2008**, *130*, 3676–3682. (c) Whited, M. T.; Grubbs, R. H. *J. Am. Chem. Soc.* **2008**, *130*, 16476–16477.

(5) Scheele, U. J.; Dechert, S.; Meyer, F. *Chem.—Eur. J.* **2008**, *14*, 5112–5115.

Chart 1



noting that redox-active elements are also ubiquitous in enzymological functions⁶ (ribonucleotide reductase,⁷ cytochrome *c* peroxidase,⁸ galactose oxidase,⁹ prostaglandin H synthase,¹⁰ lipoyl synthase,¹¹ biotin synthase,¹² diol dehydrase,¹³ pyruvate-formate lyase,¹⁴ DNA photolyase,¹⁵ and lysine-2,3-aminomutase),¹⁶ combining metal sites, in a manifold of oxidation states, and radical residues (Tyr[•], Cys[•], Gly[•], Trp[•], and TrpH^{•+}) toward executing fundamental catalytic steps (hydrogen-atom abstraction, proton transfer, and single-electron transfer).^{1,6} While electron-rich, radical-stabilizing oxygen and sulfur moieties have traditionally prevailed as research targets,^{17,18} nitrogen-centered radicals^{19,20} (NR₂[•] and NR₃^{•+}) are currently emerging as worthy competitors.

Protonation or metalation (especially with hard metal centers) of these nitrogen-centered radicals can give rise to potent electrophilic species involved, for instance, in typical olefin addition and H–atom abstraction reactions.²¹ When the metal site is redox-active, challenges arise in establishing the correct electronic state of the M–NR₂ fragment, either as a bona fide amido unit (Mⁿ⁺–NR₂[–]) or as an aminal radical-bearing moiety (M⁽ⁿ⁻¹⁾⁺–NR₂[•]).²² Wieghardt et al.’s work²³ has provided numerous instances in which the oxidation of

Chart 2

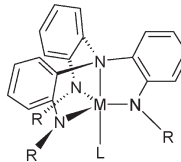
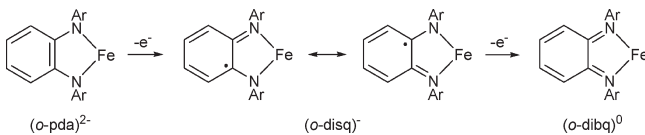


Chart 3



metal compounds with N/O/S-containing polydentate ligands has led to the storage of oxidation equivalents onto the ligand rather than the metal and has drawn attention to the care needed in correctly evaluating the role of noninnocent ligands in redox processes of a stoichiometric or catalytic nature.²⁴ However, metalloradicals involving *N*-donor moieties,²⁵ especially those that can be generated by redox processes to afford incipient *N*-centered radicals, remain scarce and require further exploration in order to understand their reactivity in the context of a rapidly growing field of nitrogen-rich ligands.

In previous work,²⁶ we have shown that tripodal reagents (M = Fe(II), Mn(II), Cr(III)), featuring the rigid triphenylamido-amine core and electron-rich aryl arms (Chart 2, R = 4-*t*-BuPh-), can be oxidized by dioxygen and other oxidants to generate a transient aminal radical at an equatorial N_{amido} atom. The metal-bound aminal radical causes rearrangement of the ligand, followed by storage of the oxidizing equivalent in a newly formed *ortho*-diiminosemiquinonato residue (*o*-disq[–], Chart 3), which can be further oxidized or reduced by one electron. In the present work, we set the stage for further exploration of the redox chemistry of ferrous tripodal compounds, by providing a whole family of reagents bearing the triphenylamido-amine core and a variety of pendant arms (R).²⁷ The ligands examined in this work are cousins of the

- (6) See contributions to thematic issue: *Chem. Rev.* **2003**, *103*, 2081–2456.
- (7) Licht, S.; Gerfen, G. J.; Stubbe, J. *Science* **1996**, *271*, 477–481.
- (8) Huyett, J. E.; Doan, P. E.; Gurbel, R.; Houseman, A. L. P.; Sivaraja, M.; Goodin, D. B.; Hoffman, B. M. *J. Am. Chem. Soc.* **1995**, *117*, 9033–9041.
- (9) Whittaker, J. W. *Adv. Biochem. Biophys.* **2005**, *433*, 227–239.
- (10) Dorlet, P.; Seibold, S. A.; Babcock, G. T.; Gerfen, G. J.; Smith, W. L.; Tsai, A. L.; Un, S. *Biochemistry* **2002**, *41*, 6107–6114.
- (11) Cicchillo, R. M.; Iwig, D. F.; Jones, A. D.; Nesbitt, N. M.; Baleanu-Gogonea, C.; Souder, M. G.; Tu, L.; Booker, S. *J. Biochemistry* **2004**, *43*, 6378–6386.
- (12) Berkovitch, F.; Nicolet, Y.; Wan, J. T.; Jarrett, J. T.; Drennan, C. L. *Science* **2004**, *303*, 76–79.
- (13) Magnusson, O. T.; Frey, P. A. *Biochemistry* **2002**, *41*, 1695–1702.
- (14) Knappe, J.; Wagner, A. F. V. *Adv. Protein Chem.* **2001**, *58*, 277–315.
- (15) Cheek, J.; Broderick, J. B. *J. Am. Chem. Soc.* **2002**, *124*, 2860–2861.
- (16) Banerjee, R. *Chem. Rev.* **2003**, *103*, 2083–2094.
- (17) (a) Miura, Y.; Tomimura, T. *Chem. Commun.* **2001**, 627–628. (b) Miura, Y.; Tomimura, T.; Teki, Y. *J. Org. Chem.* **2000**, *65*, 7889–7895.
- (18) Chaudhuri, P.; Wieghardt, K. *Prog. Inorg. Chem.* **2001**, *50*, 151–216.
- (19) (a) Merényi, G.; Lind, J. In *N-Centered Radicals*; Alsfassi, Z., Ed.; Wiley: New York, 1998; pp 599–613. (b) Maxwell, B. J.; Tsanaktsidis, J. In *N-Centered Radicals*; Alsfassi, Z., Ed.; Wiley: New York, 1998; pp 663–684.
- (20) Zard, S. Z. *Chem. Soc. Rev.* **2008**, *37*, 1603–1618.
- (21) (a) Esker, J. L.; Newcomb, M. *Adv. Heterocycl. Chem.* **1993**, *58*, 1–45. (b) Newcomb, M.; Musa, O. M.; Martinez, F. N.; Horner, J. H. *J. Am. Chem. Soc.* **1997**, *119*, 4569–4577. (c) Musa, O. M.; Horner, J. H.; Shahin, H.; Newcomb, M. *J. Am. Chem. Soc.* **1996**, *118*, 3862–3868.
- (22) (a) Gross, R.; Kaim, W. *Angew. Chem., Int. Ed.* **1985**, *24*, 856–858. (b) Kaim, W.; Wanner, M.; Knödler, A.; Zális, S. *Inorg. Chim. Acta* **2002**, *337*, 163–172.
- (23) (a) Ghosh, P.; Bill, E.; Weyhermüller, T.; Neese, F.; Wieghardt, K. *J. Am. Chem. Soc.* **2003**, *125*, 1293–1308. (b) Ghosh, P.; Bill, E.; Weyhermüller, T.; Wieghardt, K. *J. Am. Chem. Soc.* **2003**, *125*, 3967–3979. (c) Herebian, D.; Bothe, E.; Neese, F.; Weyhermüller, T.; Wieghardt, K. *J. Am. Chem. Soc.* **2003**, *125*, 9116–9128.

- (24) (a) Mukherjee, S.; Rentschler, E.; Weyhermüller, T.; Wieghardt, K.; Chaudhuri, P. *Chem. Commun.* **2003**, 1828–1829. (b) Paine, T. K.; Weyhermüller, T.; Bothe, E.; Wieghardt, K.; Chaudhuri, P. *J. Chem. Soc., Dalton Trans.* **2003**, 3136–3144.

- (25) (a) Büttner, T.; Geier, J.; Frison, G.; Harmer, J.; Calle, C.; Schweiger, A.; Schönberg, H.; Grützmacher, H. *Science* **2005**, *307*, 235–238. (b) Maire, P.; Königsmann, M.; Sreekanth, A.; Harmer, J.; Schweiger, A.; Grützmacher, H. *J. Am. Chem. Soc.* **2006**, *128*, 6578–6580. (c) Königsmann, M.; Donati, N.; Stein, D.; Schönberg, H.; Harmer, J.; Sreekanth, A.; Grützmacher, H. *Angew. Chem., Int. Ed.* **2007**, *46*, 3567–3570. (d) Donati, N.; Königsmann, M.; Stein, D.; Udino, L.; Grützmacher, H. *C. R. Chim.* **2007**, *10*, 721–730. (e) Donati, N.; Stein, D.; Büttner, T.; Schönberg, H.; Harmer, J.; Sreekanth, A.; Grützmacher, H. *Eur. J. Inorg. Chem.* **2008**, 4691–4703.

- (26) (a) Çelenligil-Çetin, R.; Paraskevopoulou, P.; Dinda, R.; Staples, R. J.; Sinn, E.; Rath, N. P.; Stavropoulos, P. *Inorg. Chem.* **2008**, *47*, 1165–1172. (b) Çelenligil-Çetin, R.; Paraskevopoulou, P.; Dinda, R.; Lalioti, N.; Sanakis, Y.; Rawashdeh, A. M.; Staples, R. J.; Sinn, E.; Stavropoulos, P. *Eur. J. Inorg. Chem.* **2008**, 673–677. (c) Çelenligil-Çetin, R.; Paraskevopoulou, P.; Lalioti, N.; Sanakis, Y.; Staples, R. J.; Rath, N. P.; Stavropoulos, P. *Inorg. Chem.* **2008**, *47*, 10998–11009.

- (27) (a) Çelenligil-Çetin, R. *Synthesis, Characterization, and Reactivity of Iron Complexes with N-Donor Ligands in Relation to Oxygenation of Hydrocarbons*, Ph.D. Thesis, Boston University, Boston, MA, **2004**. (b) Pinnapareddy, D. *Synthesis and Characterization of Metal Reagents Mediating C–X Activation (X = Cl, H) of Hydrocarbons*, Ph.D. Thesis, University of Missouri–Rolla, Rolla, MO, **2007**.

TREN family^{28–30} but, owing to the triphenylamido-amine core, are significantly more rigid and electronically variable. Depending on the arm substituents, the reagents can be infinitely tuned to display a continuum ranging from non-innocent to redox-robust ligand behavior and, thus, permit a systematic analysis of the metal/ligand synergism in supporting atom- and group-transfer chemistry. Elements of structure, characterization, and redox behavior are explored in this work, whereas aspects of reductive and oxidative reactivity will be communicated separately in due course. Parts of the present work have been previously documented in two Ph.D. theses.²⁷

Experimental Section

General Considerations. All operations were performed under anaerobic conditions under a pure dinitrogen or argon atmosphere using Schlenk techniques on an inert gas/vacuum manifold or in a drybox (O_2 , $H_2O < 1$ ppm). Anhydrous diethyl ether, methylene chloride, acetonitrile, tetrahydrofuran, hexane, pentane, benzene, toluene, dimethylformamide, dimethylacetamide, and dimethylsulfoxide were purchased from Sigma-Aldrich. Ethanol and methanol were distilled over the corresponding magnesium alkoxide, and acetone was distilled over drierite. Solvents were degassed by three freeze–pump–thaw cycles. Unless otherwise noted, all other reagents were purchased at the highest purity available. Potassium hydride was provided as a dispersion in mineral oil and was thoroughly washed prior to use with copious amounts of tetrahydrofuran followed by hexane. Compounds L^1H_3 (**1**)^{26a} L^7H_3 (**3c**)³¹ and $[K(THF)_3][L^1(Fe(II))\text{THF}] \cdot 0.5\text{THF}$ (**5**)^{26b} have been prepared according to literature methods. ^1H NMR and ^{13}C NMR spectra were recorded on Varian XL-400, Varian IN-OVA/UNITY 400 MHz, and Varian 300 Unity Plus NMR spectrometers. ^{19}F NMR spectra were recorded on a Varian Mercury spectrometer (at 188 MHz), and chemical shifts are referenced to trifluoroacetic acid (TFA, external standard). IR spectra were obtained on a Perkin-Elmer 883 IR spectrometer and FT-IR spectra on Nicolet Nexus 470 and 670 and Magna 750 FT-IR ESP spectrometers. UV–vis spectra were obtained on Hewlett-Packard 8452A diode array, Varian Cary 50, and Varian Cary 300 spectrophotometers. Electron ionization (EI) and fast-atom bombardment (FAB) mass spectra were obtained on a Finnigan MAT-90 mass spectrometer. Electrospray ionization mass spectrometry (ESI) and atmospheric pressure chemical ionization mass spectra were obtained on a Thermo-Finnigan TSQ7000 triple-quadrupole mass spectrometer, equipped with the API2 source and Performance Pack (ThermoFinnigan, San Jose, CA). HRMS data were collected on a Thermo Fisher Scientific LTQ-Orbitrap XL hybrid mass spectrometer, using the Orbitrap analyzer for acquisition of high-resolution accurate mass data. Samples were infused using the integrated syringe pump at 3 $\mu\text{L}/\text{min}$, and ionization was via the electrospray source with source settings at their defaults. In

general, settings for the ion optics were determined automatically during the regular tuning and calibration of the instrument. For high-resolution data, the Orbitrap analyzer is set to a resolution of 100 000. Microanalyses were done by Galbraith Laboratories, Knoxville, Tennessee; Quantitative Technologies Inc., Whitehouse, New Jersey; and on an in-house Perkin-Elmer 2400 CHN analyzer.

Ligand Synthesis. $[(3,5\text{-di-}tert\text{-Butyl-C}_6\text{H}_3)\text{-NH-(2-C}_6\text{H}_4)]_3\text{N}$ ($L^2\text{H}_3$, **2a**). A 250-mL Schlenk flask was charged with $(2\text{-NH}_2\text{-C}_6\text{H}_4)_3\text{N}$ (1.59 g, 5.46 mmol), 3,5-di-*tert*-butylbromobenzene (4.28 g, 16.00 mmol), and *tert*-Bu-ONa (1.78 g, 18.50 mmol). The slurry was stirred in anhydrous toluene. In another Schlenk flask, $[\text{Pd}_2(\text{dba})_3]$ (tris(dibenzylideneacetone)dipalladium, 0.075 g, 0.08 mmol) and BINAP (2,2'-bis(diphenylphosphino)-1,1'-binaphthyl, 0.150 g, 0.24 mmol) were stirred in anhydrous toluene and heated until BINAP dissolved. The resulting cherry-red solution was transferred into the former flask via a cannula. The slurry was stirred at 100 °C for 36 h to give a brown solution, with precipitation of a solid. The solution was allowed to cool to room temperature followed by the addition of diethylether. The brown solution was filtered, and the filtrate was evaporated under a vacuum to give a brown oily residue. The residue was dissolved in 10.0 mL of hexane to give a brown solution, which upon standing at room temperature gave a tan-colored solid. The solid was filtered under a vacuum and washed with a minimum amount of cold hexane. The filtrates were treated in a similar manner to obtain the product in a combined yield of 58% (2.63 g). ^1H NMR (CDCl_3 , 7.27 ppm): δ 7.22 (d, 3H, $J = 7.6$ Hz, aryl), 7.06 (m, 6H, aryl), 6.95 (t, 3H, $J = 1.6$ Hz, aryl), 6.78 (t, 3H, $J = 7.2$ Hz, aryl), 6.63 (d, 6H, $J = 1.6$ Hz, aryl), 5.89 (s, 3H, NH), 1.16 (s, 54H, *tert*-butyl). ^{13}C NMR (CDCl_3 , 77 ppm): δ 151.81, 141.89, 140.53, 134.33, 126.08, 126.38, 126.06, 116.88, 116.06, 115.85, 34.89, 31.56. IR (KBr, cm^{-1}): 3402, 3367, 3063, 2962, 2867, 1588, 1527, 1481, 1455, 1362, 1330, 1272, 1205, 1134, 1043, 977, 754, 711, 629. MS-EI (m/z) calcd: 855.31. Found: 852.4 ([M] – 3H). Elema anal. calcd for $C_{60}\text{H}_{78}\text{N}_4$: C, 84.26; H, 9.19; N, 6.55. Found: C, 84.14; H, 9.28; N, 6.47.

$[(3,5\text{-Bis-trifluoromethyl-C}_6\text{H}_3)\text{-NH-(2-C}_6\text{H}_4)]_3\text{N}$ ($L^3\text{H}_3$, **2b**). A 250-mL Schlenk flask was charged with $(2\text{-NH}_2\text{-C}_6\text{H}_4)_3\text{N}$ (1.59 g, 5.46 mmol), 3,5-bis-trifluoromethyl-bromobenzene (4.79 g, 16.38 mmol), and Cs_2CO_3 (8.15 g, 25.0 mmol). The slurry was stirred in anhydrous toluene. In another Schlenk flask, $[\text{Pd}_2(\text{dba})_3]$ (0.125 g, 0.137 mmol) and BINAP (0.255 g, 0.41 mmol) were stirred in anhydrous toluene and heated until BINAP dissolved. The resulting cherry-red solution was transferred into the former flask via a cannula. The slurry was stirred at 100 °C for 36 h to give a brown solution. At the end of the reaction, the solution was allowed to cool to room temperature, followed by the addition of diethylether. The brown solution was filtered, and the filtrate was evaporated to give a brown-black oily residue. The addition of hexane precipitated a white solid, which was filtered and recrystallized from hot hexane to afford the product as a pure crystalline solid (2.62 g, 52%). ^1H NMR (CDCl_3 , 7.27 ppm): δ 7.27 (s, 6H, aryl), 7.19 (m, 3H, aryl), 7.08 (d, 6H, $J = 4.0$ Hz, aryl), 6.84 (s, 3H, aryl), 5.46 (s, 3H, NH). ^{13}C NMR (CDCl_3 , 77 ppm): δ 144.29, 137.98, 135.03, 132.73 (q, $^2J_{\text{CF}} = 33.4$ Hz, aryl), 126.47, 125.83, 125.10, 122.90 (q, $^1J_{\text{CF}} = 272.6$ Hz, CF₃), 121.83, 115.54. ^{19}F NMR (CDCl_3 , TFA, –77 ppm): δ –63.03. IR (KBr, cm^{-1}): 3398, 3359, 3300, 3278, 3062, 1624, 1591, 1531, 1489, 1471, 1421, 1385, 1282, 1188, 1130, 999, 964, 881, 758, 729, 702, 683, 625. MS-FAB (m/z) calcd: 926.65. Found: 926.17. HRMS (ESI), m/z , [M + H]⁺ calcd. for $C_{42}\text{H}_{25}\text{N}_4\text{F}_{18}$: 927.1786. Found: 927.1788. Elema anal. calcd for $C_{42}\text{H}_{24}\text{N}_4\text{F}_{18}$: C, 54.44; H, 2.61; N, 6.05. Found: C, 54.24; H, 2.58; N, 6.17.

$[(tert\text{-Butyl-CO})\text{-NH-(2-C}_6\text{H}_4)]_3\text{N}$ ($L^4\text{H}_3$, **3a**). To a stirred solution of $(2\text{-NH}_2\text{-C}_6\text{H}_4)_3\text{N}$ (2.90 g, 10.0 mmol) and triethylamine (5.10 mL, 36.6 mmol) in THF (40 mL) was slowly added trimethylacetyl chloride (3.62 g, 30.0 mmol) at 0 °C by means of

(28) (a) Schrock, R. R. *Acc. Chem. Res.* **1997**, *30*, 9–16. (b) Verkade, J. G. *Acc. Chem. Res.* **1993**, *26*, 483–489.

(29) (a) Freundlich, J. S.; Schrock, R. R.; Davis, W. M. *J. Am. Chem. Soc.* **1996**, *118*, 3643–3655. (b) Yandulov, D. V.; Schrock, R. R. *Science* **2003**, *301*, 76–78. (c) Yandulov, D. V.; Schrock, R. R. *J. Am. Chem. Soc.* **2002**, *124*, 6252–6253. (d) Greco, G. E.; Schrock, R. R. *Inorg. Chem.* **2001**, *40*, 3850–3860. (e) Greco, G. E.; Schrock, R. R. *Inorg. Chem.* **2001**, *40*, 3861–3878. (f) Cummins, C. C.; Schrock, R. R. *Inorg. Chem.* **1994**, *33*, 395–396.

(30) (a) Parsell, T. H.; Yang, M.-Y.; Borovik, A. S. *J. Am. Chem. Soc.* **2009**, *131*, 2762–2763. (b) Lucas, R. L.; Powell, D. R.; Borovik, A. S. *J. Am. Chem. Soc.* **2005**, *127*, 11596–11597. (c) Gupta, R.; Borovik, A. S. *J. Am. Chem. Soc.* **2003**, *125*, 13234–13242. (d) MacBeth, C. E.; Golombok, A. P.; Young, V. G., Jr.; Yang, C.; Kuczera, K.; Hendrich, M. P.; Borovik, A. S. *Science* **2000**, *289*, 938–941.

(31) Jones, M. B.; MacBeth, C. E. *Inorg. Chem.* **2007**, *46*, 8117–8119.

a syringe, and the mixture was allowed to warm up to room temperature and then stirred overnight. The solvent was removed under reduced pressure, and the crude residue was purified by column chromatography with petroleum ether/ethyl acetate (3:1) to give the product as a white solid (4.34 g, 80%).³³

¹H NMR (CDCl₃, 7.27 ppm): δ 8.08 (s, 3H, NH), 7.73 (d, 3H, J = 7.6 Hz, aryl), 7.06 (t, 3H, J = 7.6 Hz, aryl), 6.97 (t, 3H, J = 7.6, aryl), 6.79 (d, 3H, J = 8.0 Hz, aryl), 0.93 (s, 27H, *tert*-butyl). ¹³C NMR (CDCl₃, 77 ppm): δ 176.42, 137.71, 131.31, 125.77, 125.46, 124.52, 124.17, 39.19, 26.98. IR (KBr, cm⁻¹): 3389, 3308, 3282, 3259, 3062, 3034, 2974, 2960, 2909, 2869, 1680, 1653, 1591, 1516, 1492, 1480, 1439, 1396, 1365, 1302, 1264, 1228, 1161, 1115, 1052, 1028, 930, 771, 757, 733, 624, 490, 478. MS-FAB (*m/z*) calcd: 542.33. Found: 542.32. Elem anal. calcd for C₃₃H₄₂N₄O₃: C, 73.03; H, 7.80; N, 10.32. Found: C, 72.94; H, 7.68; N, 10.54.

[3,5-Dichloro-C₆H₃]-NH-(2-C₆H₄)₃N (L⁵H₃, 2c). A mixture of BINAP (0.089 g, 0.15 mmol), [Pd₂(dba)₃] (0.046 g, 0.05 mmol), and Cs₂CO₃ (3.26 g, 10 mmol) was stirred in 10.0 mL of anhydrous toluene at ambient temperature for 30 min in a 50.0 mL Schlenk flask in the drybox. To this mixture were added 1-bromo-3,5-dichloro-benzene (1.36 g, 6.0 mmol) and (2-NH₂-C₆H₄)₃N (0.58 g, 2.0 mmol). The flask was attached to a Schlenk line, and the mixture was heated under reflux under a nitrogen atmosphere for 42 h. The mixture was then allowed to cool down to room temperature and filtered under a vacuum. The solution was concentrated under a vacuum, and the residue was purified by column chromatography on silica gel (ethyl acetate/petroleum ether = 1:20) to afford the product as a pale yellow solid. The solid was recrystallized from chloroform/hexane to afford pure product as a white solid (0.834 g, 1.15 mmol) in 57.5% isolated yield. ¹H NMR (CDCl₃, 7.24 ppm): δ 7.30 (d, 6H, J = 7.6 Hz, aryl), 7.13–7.18 (m, 3H, aryl), 7.00–7.02 (m, 6H, aryl), 6.78 (t, 3H, J = 1.6 Hz, aryl), 6.38 (d, 6H, J = 1.6 Hz, aryl), 5.25 (s, 3H, NH). ¹³C NMR (CDCl₃, 77 ppm): δ 144.88, 137.78, 135.66, 126.26, 125.87, 124.25, 121.79, 120.70, 114.56. IR (KBr, cm⁻¹): 3395, 1578, 1505, 1468, 1442, 1306, 1253, 1109, 987, 954, 829, 759, 756, 657, 563. MS-FAB (*m/z*) calcd: 722.01. Found: 722.01. HRMS (ESI), *m/z* [M]⁺ calcd. for C₃₆H₂₄N₄Cl₆: 722.0127. Found: 722.0130. Elem anal. calcd for C₃₆H₂₄N₄Cl₆: C, 59.61; H, 3.34; N, 7.72. Found: C, 59.44; H, 3.38; N, 7.61.

[Phenyl-CO]-NH-(2-C₆H₄)₃N (L⁶H₃, 3b). To a stirred solution of (2-NH₂-C₆H₄)₃N (2.90 g, 10.0 mmol) and triethylamine (5.10 mL, 36.6 mmol) in THF (35 mL) was slowly added benzoyl chloride (4.22 g, 30.0 mmol) at 0 °C by means of a syringe, and the mixture was allowed to warm up to room temperature and then stirred overnight. The solvent was removed under reduced pressure, and the crude residue was purified by recrystallization from hexane/ethyl acetate (10:1) to give the product as a white solid (5.37 g, 89%). ¹H NMR (CDCl₃, 7.24 ppm): δ 8.82 (s, 3H, NH), 7.57 (m, 3H, aryl), 7.42 (m, 9H, aryl), 7.24 (t, 6H, J = 7.6 Hz, aryl), 6.97 (m, 9H, aryl). ¹³C NMR (CDCl₃, 77 ppm): δ 165.54, 137.96, 133.77, 131.50, 131.10, 127.97, 127.13, 126.27, 125.73, 124.79, 124.29. IR (KBr, cm⁻¹): 3350, 3277, 3058, 3025, 1674, 1660, 1638, 1597, 1578, 1525, 1490, 1477, 1453, 1438, 1311, 1263, 1160, 1121, 1073, 1047, 1025, 946, 926, 902, 828, 797, 756, 715, 700, 688, 624, 592, 496, 477. MS-FAB (*m/z*) calcd: 602.23. Found: 603.23 ([M + H]⁺). HRMS (ESI), *m/z* [M]⁺ calcd. for C₃₉H₃₁N₄O₃: 603.2391. Found: 603.2393. Elem anal. calcd for C₃₉H₃₀N₄O₃: C, 77.72; H, 5.02; N, 9.30. Found: C, 77.84; H, 5.08; N, 9.44.

(32) (a) Hartwig, J. F.; Kawatsura, M.; Hauck, S. I.; Shaughnessy, K. H.; Alcazar-Roman, L. M. *J. Org. Chem.* **1999**, *64*, 5575–5580. (b) Wolfe, J. P.; Buchwald, S. L. *J. Org. Chem.* **2000**, *65*, 1144–1157.

(33) A new synthesis of ligand L⁴H₃ appeared in the literature while this manuscript was in an advanced stage of preparation. A previous synthesis was communicated in ref^{27b}; Jones, M. B.; Hardcastle, K. I.; MacBeth, C. E. *Polyhedron* **2009**, DOI: 10.1016/j.poly.2009.06.013.

[(CF₃CO)-NH-(2-C₆H₄)₃N (L⁸H₃, 3d). To a stirred solution of (2-NH₂-C₆H₄)₃N (2.90 g, 10.0 mmol) and triethylamine (5.10 mL, 36.6 mmol) in THF (40 mL) was slowly added trifluoroacetic anhydride (4.17 mL, 30.0 mmol) at 0 °C, and the mixture was allowed to warm up to room temperature and then stirred overnight. The solvent was removed under reduced pressure, and the crude residue was purified by column chromatography with petroleum ether/ethyl acetate (3:1) to give the product as a white solid (5.09 g, 88%). Colorless crystals suitable for X-ray structural analysis were grown from acetonitrile at room temperature. ¹H NMR (CDCl₃, 7.27 ppm): δ 8.61 (s, 3H, NH), 7.65 (d, 3H, J = 6.8 Hz, aryl), 7.21 (m, 6H, aryl), 6.86 (d, 3H, J = 15.6 Hz, aryl). ¹³C NMR (CDCl₃, 77 ppm): δ 154.93 (q, ²J_{CF} = 37.9 Hz, C(O)CF₃), 138.05, 128.51, 127.75, 126.28, 125.97, 124.31, 115.37 (q, ¹J_{CF} = 288.5 Hz, CF₃). ¹⁹F NMR (CDCl₃, TFA, -77 ppm): δ -75.13. IR (KBr, cm⁻¹): 3266, 3136, 3070, 1727, 1703, 1540, 1287, 909, 759. HRMS (ESI), *m/z*, [M]⁺ calcd. for C₂₄H₁₆N₄F₉O₃: 579.1073. Found: 579.1071. Calcd for C₂₄H₁₅N₄F₉O₃: C, 49.84; H, 2.61; N, 9.69. Found: C, 49.88; H, 2.57; N, 9.44.

[iso-Propyl-NH-(2-C₆H₄)₃N (L⁹H₃, 4). In an ACE pressure tube under an inert atmosphere, Shvo's catalyst (0.16 g, 0.15 mmol) and (2-NH₂-C₆H₄)₃N (2.90 g, 10.0 mmol) were dissolved in toluene (7.25 mL) and isopropylamine (5.11 mL, 60.0 mmol). The pressure tube was then heated at 150 °C for 24 h in an oil bath. The solvent was removed in vacuo, and the crude product was purified by column chromatography with petroleum ether/ethyl acetate (100:1) as an eluent to afford the product as a white solid (3.75 g, 90%). Colorless crystals suitable for X-ray structural analysis were grown from acetonitrile at room temperature. ¹H NMR (CDCl₃, 7.24 ppm): δ 6.99 (td, *J* = 7.8 Hz, *J* = 1.6 Hz, 3H, aryl), 6.87 (dd, *J* = 7.8 Hz, *J* = 1.6 Hz, 3H, aryl), 6.61 (dd, *J* = 7.8 Hz, *J* = 1.2 Hz, 2H, aryl), 6.53 (td, *J* = 7.8 Hz, *J* = 1.2 Hz, 4H, aryl), 3.78 (d, *J* = 8.0 Hz, 3H, NH), 3.52 (m, 3H, CHMe₂), 0.95 (br, 18H, CHMe₂). ¹³C NMR (CD₃Cl, 77 ppm): δ 142.37, 132.31, 125.66, 125.53, 116.19, 111.33, 43.61, 22.81. IR (KBr, cm⁻¹): 3266, 3136, 3070, 1727, 1703, 1541, 1287, 1154, 909, 758. HRMS (ESI), *m/z*, [M]⁺ calcd. for C₂₇H₃₇N₄: 417.3013. Found: 417.3012. Calcd. for C₂₇H₃₆N₄: C, 77.84; H, 8.71; N, 13.45. Found: C, 77.54; H, 8.61; N, 13.63.

Synthesis of Ferrous Complexes. [K(THF)₃][L²Fe(II)-THF] (6). The ligand L²H₃ (0.285 g, 0.33 mmol) was dissolved in degassed THF (15 mL), and KH (0.040 g, 1.0 mmol) was added to this solution. The mixture was allowed to stir overnight, followed by the addition of anhydrous FeCl₂ (0.042 g, 0.33 mmol). This mixture was stirred for an additional 12 h to afford a dark yellow-brown solution. The solution was filtered, and the filtrate was reduced under a vacuum to 3.0 mL. Pentane (20 mL) was carefully layered over the THF, and the system was allowed to slowly mix at -30 °C to afford yellow-brown crystalline material of the title compound (0.235 g, 58%). Crystals suitable for X-ray analysis can be obtained as long yellow-brown needles from concentrated THF solutions. ¹H NMR (CD₃CN, 1.95 ppm): δ 47.28, 36.23, 31.93, 18.67, 13.60, 8.23, 7.6–6.46, 6.05, 3.66, 2.12, 1.82, 1.22, 1.17, 0.22, -1.82, -2.98, -8.56, -23.43, -26.76, -32.20. IR (KBr, cm⁻¹): 3385, 3043, 2954, 2895, 2859, 1579, 1474, 1442, 1427, 1388, 1358, 1326, 1307, 1275, 1244, 1200, 1153, 1123, 1109, 1039, 995, 972, 902, 861, 849, 744, 707, 620. UV-vis (THF): λ_{max} (ε (M⁻¹ cm⁻¹)) 368 (23 000). Elem anal. calcd for C₇₆H₁₀₇N₄FeKO₄: C, 73.87; H, 8.73; N, 4.53. Found: C, 74.11; H, 8.68; N, 4.59.

[K(THF)₂][L³Fe(II)-THF] (7). The ligand L³H₃ (0.400 g, 0.43 mmol) was dissolved in degassed THF (30 mL), and KH (0.052 g, 1.3 mmol) was added to this solution. The mixture was allowed to stir overnight, followed by the addition of anhydrous FeCl₂ (0.055 g, 0.43 mmol). This mixture was stirred for an additional 12 h to afford a dark yellow-brown solution. The solvent was reduced under a vacuum to 10.0 mL, and the solution was refrigerated (-30 °C) overnight. The insoluble

salts were filtered off on an anaerobic frit in the drybox, and the filtrate was further reduced to 5.0 mL. Pentane (20 mL) is carefully layered over the THF, and the system is allowed to slowly mix at -30°C to afford yellow-brown crystalline material of the title compound (0.330 g, 62%). Crystals suitable for X-ray diffraction are obtained by the slow diffusion of pentane into concentrated THF solutions of the bulk material at -30°C . ^1H NMR (CD_3CN , 1.95 ppm): δ 32.82, 15.66, 7.20, 7.05, 6.83, 3.65, 1.80, -1.82, -5.27, -29.41, -35.00. IR (KBr, cm^{-1}): 3385, 3049, 2966, 2872, 1618, 1587, 1518, 1477, 1412, 1379, 1274, 1172, 1128, 1042, 995, 959, 869, 858, 754, 727, 701, 682, 665, 623. UV-vis (THF): λ_{\max} (ϵ ($\text{M}^{-1} \text{cm}^{-1}$)): 339 (38 000). Elem anal. calcd for $\text{C}_{54}\text{H}_{45}\text{N}_4\text{F}_{18}\text{FeKO}_3$: C, 52.52; H, 3.67; N, 4.54. Found: C, 52.28; H, 3.56; N, 4.34.

[K(DMA)₂][L⁴Fe(II)] (8). The ligand L⁴H₃ (0.398 g, 0.73 mmol) was dissolved in degassed DMA (10 mL), and KH (0.088 g, 2.19 mmol) was added to this solution. The mixture was allowed to stir overnight, followed by the addition of anhydrous FeCl₂ (0.093 g, 0.73 mmol). This mixture was stirred for an additional 12 h to afford a light green-brown solution. The solution was refrigerated (-30°C) overnight, and the insoluble salts were filtered off on an anaerobic frit in the drybox. Diethyl ether (20 mL) was carefully layered over the DMA solution, and the system is allowed to slowly mix at -30°C to afford light brown crystalline material of the title compound as sticky crystalline material suitable for X-ray diffraction (0.290 g, 48.9%). ^1H NMR (CD_3CN , 1.95 ppm): δ 56.77, 47.85, 34.92, 20.95, 19.70, 13.12, 12.49, 11.97, 11.69, 7.99, 7.65, 7.53, 6.92, 6.59, 2.97, 2.84, 1.98, 0.91, -3.00, -10.82, -14.80. IR (KBr, cm^{-1}): 3266, 3048, 2943, 2916, 2859, 1634, 1591, 1557, 1534, 1473, 1442, 1389, 1338, 1311, 1265, 1240, 1212, 1169, 1106, 1037, 1014, 958, 931, 914, 752, 626, 589. UV-vis (THF): λ_{\max} (ϵ ($\text{M}^{-1} \text{cm}^{-1}$)) 294 (14 000). Elem anal. calcd for $\text{C}_{41}\text{H}_{57}\text{N}_6\text{FeKO}_5$: C, 60.88; H, 7.10; N, 10.39. Found: C, 60.48; H, 7.21; N, 10.52.

[K(L⁵)Fe(II)-THF] (9). The ligand L⁵H₃ (0.354 g, 0.49 mmol) was dissolved in degassed THF (30 mL), and KH (0.059 g, 1.47 mmol) was added to this solution. The mixture was allowed to stir overnight, followed by the addition of anhydrous FeCl₂ (0.062 g, 0.49 mmol). This mixture was stirred for an additional 12 h to afford a light green-brown solution. The solvent was reduced under a vacuum to 10.0 mL, and the solution was refrigerated (-30°C) overnight. The insoluble salts were filtered off on an anaerobic frit in the drybox, and the filtrate was further reduced to 5.0 mL. Pentane (20 mL) is carefully layered over the THF, and the system is allowed to slowly mix at -30°C to afford off-white crystalline material of the title compound (0.380 g, 87%). Essentially colorless crystals suitable for X-ray diffraction are obtained by the slow diffusion of pentane into concentrated THF solutions of the bulk material at -30°C . ^1H NMR (CD_3CN , 1.95 ppm): δ 15.60, 7.25, 6.88, 6.61, 3.65, 1.81, -1.91, -5.10. IR (KBr, cm^{-1}): 3621, 3386, 3051, 2968, 2868, 1578, 1504, 1473, 1440, 1309, 1275, 1255, 1156, 1109, 1064, 1042, 987, 978, 954, 831, 794, 756, 76, 705, 665, 657, 622, 469, 430. UV-vis (THF): λ_{\max} (ϵ ($\text{M}^{-1} \text{cm}^{-1}$)) 374 (25 000). Elem anal. calcd for $\text{C}_{40}\text{H}_{29}\text{N}_4\text{Cl}_6\text{FeKO}$: C, 54.02; H, 3.29; N, 6.30. Found: C, 54.18; H, 3.26; N, 6.48.

[K₂(THF)₅][L⁶Fe(II)₂] · 2THF (10). The ligand L⁶H₃ (0.323 g, 0.54 mmol) was dissolved in degassed THF (30 mL), and KH (0.065 g, 1.62 mmol) was added to this solution. The mixture was allowed to stir overnight, followed by the addition of anhydrous FeCl₂ (0.068 g, 0.54 mmol). This mixture was stirred for an additional 12 h to afford a yellow-orange solution. The solvent was reduced under a vacuum to 10.0 mL, and the solution was refrigerated (-30°C) overnight. The insoluble salts were filtered off on an anaerobic frit in the drybox, and the filtrate was further reduced to 5.0 mL and refrigerated at -30°C . Large yellow-orange crystals (0.264 g, 52%), suitable for X-ray analysis, were deposited from the THF solution after several days. ^1H NMR ($d^6\text{-THF}$, 1.73, 3.58 ppm): δ 7.80 (t, 3H, $J=4.7$ Hz, aryl), 7.49 (d,

6H, $J=8.3$ Hz, aryl), 7.35 (t, 3H, $J=6.8$ Hz, aryl), 7.20 (t, 6H, $J=7.1$ Hz, aryl), 7.04 (t, 6H, $J=3.6$ Hz, aryl), 6.92 (m, 3H, aryl). IR (KBr, cm^{-1}): 3049, 3016, 2970, 2865, 1523, 1477, 1445, 1379, 1309, 1257, 1130, 1090, 928, 899, 793, 752, 703, 621, 585, 416. UV-vis (THF): λ_{\max} (ϵ ($\text{M}^{-1} \text{cm}^{-1}$))) 290 (sh). Elem anal. calcd for $\text{C}_{106}\text{H}_{110}\text{N}_8\text{Fe}_2\text{K}_2\text{O}_{13}$: C, 67.22; H, 5.85; N, 5.92. Found: C, 67.47; H, 5.91; N, 5.84.

[K(NCMe)][L⁶Fe(II)-NCMe] · 2MeCN (11). The ligand L⁶H₃ (0.242 g, 0.40 mmol) was dissolved in degassed THF (30 mL), and KH (0.048 g, 1.20 mmol) was added to this solution. The mixture was allowed to stir overnight, followed by the addition of anhydrous FeCl₂ (0.051 g, 0.40 mmol). This mixture was stirred for an additional 12 h to afford a yellow-orange solution. The solvent was reduced under a vacuum to 10.0 mL, and the solution was refrigerated (-30°C) overnight. The insoluble salts were filtered off on an anaerobic frit in the drybox, and the filtrate was evaporated under a vacuum to dryness. The residue was dissolved in MeCN (30 mL); the yellow solution was filtered and reduced to 10.0 mL. Yellow-orange crystals (0.222 g, 65%), suitable for X-ray analysis, were deposited from the MeCN solution overnight. ^1H NMR (CD_3CN , 1.95 ppm): δ 28.28, 13.93, 12.66, 7.59, 7.60–7.42, 7.38, 7.36, 7.33, 7.23, 7.21, 7.18, 6.93, 6.92, 6.81, 6.79, 6.78, 6.66, 5.71, 4.93, 3.04, 2.10, 1.98, 1.29. IR (KBr, cm^{-1}): 3047, 3014, 2915, 2847, 1593, 1579, 1554, 1473, 1442, 1371, 1241, 1157, 1131, 1093, 1069, 1038, 1022, 929, 796, 755, 722, 699, 621, 593. UV-vis (MeCN): λ_{\max} (ϵ ($\text{M}^{-1} \text{cm}^{-1}$))) 271 (49500). Elem anal. calcd for $\text{C}_{47}\text{H}_{39}\text{N}_8\text{FeKO}_3$: C, 65.73; H, 4.58; N, 13.05. Found: C, 65.49; H, 4.66; N, 13.33.

[K₂(DMA)₄][K(L⁷)₂Fe(II)₂] · 2DMA (12). The ligand L⁷H₃ (0.274 g, 0.55 mmol) was dissolved in degassed DMA (10 mL), and KH (0.066 g, 1.65 mmol) was added to this solution. The mixture was allowed to stir overnight, followed by addition of anhydrous FeCl₂ (0.070 g, 0.55 mmol). This mixture was stirred for an additional twelve hours to afford a yellow-brown solution. The solution was refrigerated (-30°C) overnight, and the insoluble salts were filtered off on an anaerobic frit in the Drybox. Diethyl ether (20 mL) was carefully layered over the DMA solution, followed by 10 mL of pentane, and the system was allowed to slowly mix at -30°C to afford light yellow crystalline material of the title compound, which is suitable for X-ray diffraction (0.265 g, 67%). ^1H NMR (CD_3CN , 1.95 ppm): δ 7.72 (d, 12H, $J=7.5$ Hz, aryl), 7.12 (td, 12H, $J=1.5$ Hz, $J=7.3$ Hz, aryl), 7.05 (td, 12H, $J=1.5$ Hz, $J=7.3$ Hz, aryl), 6.72 (d, 12H, $J=7.6$ Hz, aryl), 2.94 (s, 18H, DMA), 2.81 (s, 18H, DMA), 2.21 (sept, 12H, $J=6.7$ Hz, CH), 1.97 (s, DMA), 0.93 (s, 36H, CH_3), 1.51 (s, 36H, CH_3). IR (KBr, cm^{-1}): 3615, 3225, 3174, 3105, 3048, 3017, 2958, 2923, 2862, 1636, 1588, 1541, 1515, 1477, 1443, 1410, 1393, 1304, 1258, 1216, 1196, 1159, 1089, 1034, 1014, 963, 944, 914, 887, 745, 621, 590, 548, 486, 476. UV-vis (MeCN): λ_{\max} (ϵ ($\text{M}^{-1} \text{cm}^{-1}$))) 293 (53 000). Elem anal. calcd for $\text{C}_{144}\text{H}_{186}\text{N}_{22}\text{Fe}_4\text{K}_4\text{O}_{18}$: C, 59.78; H, 6.48; N, 10.65; Fe 7.72. Found: C, 59.42; H, 6.46; N, 10.53, Fe 7.78.

[K(DMA)][L⁸Fe(II)-DMA] (13) and [K(NCMe)][L⁸Fe(II)-NCMe] (14). The ligand L⁸H₃ (0.250 g, 0.43 mmol) was dissolved in degassed DMA (10 mL), and KH (0.052 g, 1.30 mmol) was added to this solution. The mixture was allowed to stir overnight, followed by the addition of anhydrous FeCl₂ (0.055 g, 0.43 mmol). This mixture was stirred for an additional 12 h to afford a light yellow-brown solution. The solution was refrigerated (-30°C) overnight, and the insoluble salts were filtered off on an anaerobic frit in the drybox. Diethyl ether (20 mL) was carefully layered over the DMA solution, and the system was allowed to slowly mix at -30°C to afford off-white crystalline material of the title compound (0.212 g, 58%). Crystals suitable for X-ray diffraction analysis were obtained from slow diffusion of diethyl ether into concentrated DMA solutions of the compound. ^1H NMR ($\text{CD}_3\text{C}(\text{O})\text{N}(\text{CD}_3)_2$, 2.10 ppm): δ 7.66, 7.31, 6.98, 3.14, 2.97, 2.10. IR (KBr, cm^{-1}): 3487, 3061, 3019, 2928,

2869, 1726, 1627, 1483, 1453, 1402, 1258, 1163, 1019, 966, 756, 726, 594. UV-vis (DMA): λ_{max} 286 (sh). Elem anal. calcd for $C_{32}H_{30}N_6F_9FeKO_5$: C, 45.51; H, 3.58; N, 9.95. Found: C, 45.23; H, 3.47; N, 9.77.

The acetonitrile adduct **14** was synthesized by dissolving **13** in MeCN, filtering, and concentrating the solution to saturation. Colorless crystals of the compound were obtained overnight at -30°C (85%). ^1H NMR (CD_3CN , 1.95 ppm): δ 20.64, 11.19, 2.74. IR (KBr, cm^{-1}): 3431, 3057, 3021, 2994, 2929, 2579, 2307, 2281, 2255, 1630, 1587, 1478, 1451, 1416, 1368, 1303, 1253, 1225, 1146, 1104, 1035, 949, 938, 870, 865, 824, 773, 762, 746, 727, 697, 665, 626, 611, 560, 496, 464, 428, 418. UV-vis (MeCN): λ_{max} (ϵ ($M^{-1} \text{ cm}^{-1}$)) 250 (35 700). Elem anal. calcd For $C_{28}H_{18}N_6F_9FeKO_3$: C, 44.70; H, 2.41; N, 11.17. Found: C, 44.52; H, 2.44; N, 11.32.

[K(L⁹)Fe(II)]₂ (**15**). The ligand $L^9\text{H}_3$ (0.223 g, 0.54 mmol) was dissolved in degassed THF (30 mL), and KH (0.065 g, 1.62 mmol) was added to this solution. The mixture was allowed to stir overnight, followed by the addition of anhydrous FeCl_2 (0.068 g, 0.54 mmol). This mixture was stirred for an additional 12 h to afford a green-brown solution. The solvent was reduced under a vacuum to 10.0 mL, and the solution was refrigerated (-30°C) overnight. The insoluble salts and a green-brown oily residue were filtered off on an anaerobic frit in the drybox, and the orange filtrate was further reduced to 5.0 mL. Pentane (20 mL) is carefully layered over the THF, and the system is allowed to slowly mix at -30°C to afford orange crystalline material of the title compound (0.140 g, 51%). Crystals suitable for X-ray diffraction are obtained by the slow diffusion of pentane into concentrated THF solutions of the bulk material at -30°C . ^1H NMR (CD_3CN , 1.95 ppm): δ 68.00, 50.22, 46.12, 41.68, 35.32, 6.90, 6.84, 3.65, 2.96, 2.84, 2.22, 1.81, -7.22, -8.15, -14.62, -26.22. IR (KBr, cm^{-1}): 3490, 3386, 3054, 3026, 2955, 2919, 2860, 1595, 1580, 1510, 1461, 1433, 1380, 1361, 1316, 1260, 1228, 1173, 1153, 1120, 1042, 740, 626, 576, 417. UV-vis (THF): λ_{max} (ϵ ($M^{-1} \text{ cm}^{-1}$)) 313 (23 000). Elem anal. calcd for $C_{54}H_{66}N_8Fe_2K_2$: C, 63.77; H, 6.54; N, 11.02. Found: C, 63.53; H, 6.47; N, 10.94.

Other Physical Measurements. Cyclic voltammetry was carried out with an Eco Chemie Autolab PGSTAT100 electrochemical workstation fitted in a drybox and controlled with the General Purpose Electrochemical Software or with a Bipotentiostat AFCBP1 from Pine Instrument Company fitted in a drybox and controlled with the PineChem 2.7.9 software. Experiments were performed using a gold disk working electrode (2 mm diameter) and a Ag/Ag^+ (0.01 M AgNO_3 and 0.1 or 0.5 M [$^7\text{Bu}_4\text{N}$]PF₆ in acetonitrile or DMSO) nonaqueous reference electrode (Bioanalytical Systems, Inc.) with a prolonged bridge (0.1 or 0.5 M [$^7\text{Bu}_4\text{N}$]PF₆ in acetonitrile or DMSO). A thin Pt foil or gauge (8 cm^2 , Sigma-Aldrich) was employed as counterelectrode. The working electrode was polished using successively 6, 3, and 1 μm diamond paste on a DP-Nap polishing cloth (Struers, Westlake, OH), washed with water and acetone, and air-dried. The Pt foil and gauge electrodes were cleaned in a $\text{H}_2\text{O}_2/\text{H}_2\text{SO}_4$ (conc) solution (1:4 v/v) and oven-dried. The concentrations of the samples were between 1 and 3 mM, and that of [$^7\text{Bu}_4\text{N}$]PF₆ (supporting electrolyte) was 0.1 or 0.5 M. The potential sweep rate varied between 10–1000 mV/s. All potentials are reported versus the ferrocenium/ferrocene (Fc^+/Fc) couple.

Mössbauer measurements were recorded on a constant acceleration conventional spectrometer with a source of ^{57}Co (Rh matrix) located at the Institute of Materials Science, NCSR “Demokritos”, Greece. Variable-temperature spectra were obtained by using an Oxford cryostat. Isomer shift values are quoted relative to iron foil at 293 K.

Crystallographic data were collected at the Departments of Chemistry at Harvard University, Missouri University of Science and Technology, University of Missouri–Columbia,

and University of Missouri–St. Louis by using a Bruker SMART CCD (charge-coupled device)-based diffractometer equipped with an Oxford Cryostream low-temperature apparatus operating at variable low temperatures. A suitable crystal was chosen and mounted on a glass fiber using grease. Data were measured using ω scans of 0.3° per frame for 30 s, such that a hemisphere was collected. A total of 1271 frames were collected with a maximum resolution of 0.75 Å. The first 50 frames were re-collected at the end of data collection to monitor for decay. Cell parameters were retrieved using SMART software and refined using SAINT on all observed reflections. Data reduction was performed using the SAINT software, which corrects for Lp and decay. The structures are solved by the direct method using the SHELXS-97 program and refined by the least-squares method on F², SHELXL-97, incorporated in SHELXTL-PC V 5.10. All non-hydrogen atoms were refined anisotropically. Hydrogens were calculated by geometrical methods and refined as a riding model. The crystals used for diffraction studies showed no decomposition during data collection. All drawings are done at 30% ellipsoids unless otherwise stated. Pertinent crystallographic data are collected in Tables 1 (compounds **6–15**) and S1 (compounds **2a**, **3a–d**, **4**; Supporting Information). Selected bond distances and angles for compounds **6–15** are given in Tables 2 and 3, respectively.

Results and Discussion

Ligand Synthesis. Scheme 1 summarizes the ligands employed in the present study. Their synthesis (Scheme 2) makes use of a common precursor, 2,2',2''-triaminotriphenylamine ($L\text{H}_3$), previously reported by us,^{26a} and by MacBeth and Jones³¹ in a more concise preparation. Aryl, acyl, and alkyl arms are then appended to the *ortho*-NH₂ moieties via a variety of C–N coupling methodologies.

Aryl arms can be readily installed according to the general Hartwig-Buchwald, Pd-mediated, coupling methodology for the arylation of amines.³² Substituents at aryl positions 4- (**1**) and 3,5- (**2**) can be easily accommodated to afford a series of electronically and sterically diverse variants (Scheme 2). The electron-rich ligand **1** has been previously reported²⁶ and shown to engage in oxidative ligand rearrangement in several Fe(II), Mn(II), and Cr(III) complexes.

Acyl arms can be attached via straightforward condensations of the aniline –NH₂ moieties with acyl chlorides or anhydrides in the presence of a base (**3**, Scheme 2). Better yields are obtained by using Et₃N in organic solvents rather than NaOH in aqueous media. The former method was employed by MacBeth and Jones in the synthesis of the previously reported ligand $L^9\text{H}_3$.³¹ Alkyl arms proved to be the most difficult to append but are amenable to installation via condensation of the aniline –NH₂ units with alkylamines, mediated by Shvo's catalyst³⁴ (**4**, Scheme 2). The procedure, which leads to ammonia formation, was pioneered by Beller et al.³⁵ and is applicable only to alkylamines possessing α -H atoms, by means of the “borrowing hydrogen” methodology.³⁶ A single example with *iso*-propyl substituents is

(34) (a) Karvembu, R.; Prabhakaran, R.; Natarajan, N. *Coord. Chem. Rev.* **2005**, *249*, 911–918. (b) Prabhakaran, R. *Synlett* **2004**, 2048–2049.

(35) Hollmann, D.; Bähn, S.; Tillack, A.; Beller, M. *Angew. Chem., Int. Ed.* **2007**, *46*, 8291–8294.

(36) Hamid, M. H. S. A.; Allen, C. L.; Lamb, G. W.; Maxwell, A. C.; Maytum, H. C.; Watson, A. J. A.; Williams, J. M. J. *J. Am. Chem. Soc.* **2009**, *131*, 1766–1774.

Table 1. Summary of Crystallographic Data for Fe(II) Compounds 6–15

	6	7	8	9	10
formula	C ₇₆ H ₁₀₇ FeKN ₄ O ₄	C ₅₄ H ₄₅ F ₁₈ FeKN ₄ O ₃	C ₄₁ H ₅₇ FeKN ₆ O ₅	C ₄₀ H ₂₉ Cl ₆ FeKN ₄ O	C ₂₁₂ H ₂₂₀ Fe ₄ K ₄ N ₁₆ O ₂₆
M _r	1235.61	1234.89	808.88	889.32	3787.84
cryst syst	monoclinic	triclinic	triclinic	monoclinic	triclinic
space group	P2(1)/n	P <bar{1}< td=""><td>P<bar{1}< td=""><td>C2/c</td><td>P<bar{1}< td=""></bar{1}<></td></bar{1}<></td></bar{1}<>	P <bar{1}< td=""><td>C2/c</td><td>P<bar{1}< td=""></bar{1}<></td></bar{1}<>	C2/c	P <bar{1}< td=""></bar{1}<>
a (Å)	13.683(2)	12.732(4)	11.054(4)	27.8793(15)	13.4826(12)
b (Å)	35.079(5)	14.506(4)	11.624(4)	13.0277(7)	14.9649(15)
c (Å)	15.003(2)	16.574(5)	17.167(6)	21.2649(11)	23.685(2)
α (deg)	90	111.680(6)	101.488(6)	90	80.439(6)
β (deg)	100.479(2)	92.961(6)	91.197(6)	102.3540(10)	85.325(6)
γ (deg)	90	98.996(5)	95.524(6)	90	79.324(6)
V (Å ³)	7081.1(18)	2789.7(14)	2149.77	7544.6(7)	4624.6(7)
Z	4	2	2	8	1
D _{calcd} (g cm ⁻³)	1.159	1.470	1.250	1.566	1.360
T (K)	130(2)	223(2)	223(2)	130(2)	100(2)
λ (Å)	0.71073	0.71073	0.71073	0.71073	0.71073
μ (mm ⁻¹)	0.321	0.451	0.496	0.975	0.473
R ₁ ^a (I > 2σ(I))	0.0870	0.1170	0.0791	0.0389	0.1385
wR ₂ ^b (I > 2σ(I))	0.1819	0.2760	0.2142	0.1048	0.3259

11	12	13	14	15	
formula	C ₄₇ H ₃₉ FeKN ₈ O ₃	C ₁₄₄ H ₁₈₆ Fe ₄ K ₄ N ₂₂ O ₁₈	C ₃₂ H ₃₀ F ₉ FeKN ₆ O ₅	C ₂₈ H ₁₈ F ₉ FeKN ₆ O ₃	C ₅₄ H ₆₆ Fe ₂ K ₂ N ₈
M _r	858.81	2892.95	844.57	752.43	1017.05
cryst syst	monoclinic	triclinic	monoclinic	monoclinic	triclinic
space group	P2(1)/n	P <bar{1}< td=""><td>Cc</td><td>P2(1)/c</td><td>P<bar{1}< td=""></bar{1}<></td></bar{1}<>	Cc	P2(1)/c	P <bar{1}< td=""></bar{1}<>
a (Å)	10.208(3)	20.365(3)	18.2046(14)	10.6910(18)	9.520(3)
b (Å)	23.532(7)	20.450(3)	10.7576(8)	18.772(4)	13.226(4)
c (Å)	18.691(5)	21.442(3)	19.0952(15)	15.681(3)	20.248(6)
α (deg)	90	64.440(2)	90	90	89.225(5)
β (deg)	103.422(5)	81.256(2)	94.4560(10)	101.933(5)	80.427(5)
γ (deg)	90	67.663(2)	90	90	86.355(5)
V (Å ³)	4367(2)	7450.8(19)	3728.3(5)	3079.0(10)	2508.9(12)
Z	4	2	4	4	2
D _{calcd} (g cm ⁻³)	1.306	1.289	1.505	1.623	1.346
T (K)	223(2)	130(2)	130(2)	130(2)	130(2)
λ (Å)	0.71073	0.71073	0.71073	0.71073	0.71073
μ (mm ⁻¹)	0.491	0.562	0.608	0.721	0.789
R ₁ ^a (I > 2σ(I))	0.0672	0.0786	0.0715	0.0707	0.0754
wR ₂ ^b (I > 2σ(I))	0.1497	0.1917	0.1887	0.1425	0.1520

^a R₁ = $\sum |F_o| - |F_c| / \sum |F_o|$. ^b wR₂ = $[\sum w(F_o^2 - F_c^2)^2 / \sum w(F_o^2)]^{1/2}$.

Table 2. Selected Interatomic Distances (Å) for Compounds 6–15

	6	7	8	9	10	11	12	13	14	15
Fe(1)–N(1)	2.244(3)	2.301(6)	2.203(3)	2.2246(17)	2.459(n.b.)	2.280(3)	2.506(n.b.)	2.437(5)	2.378(4)	2.132(6)
Fe(1)–N(2)	2.063(3)	2.050(7)	3.350(nb)	2.0808(18)	2.083(10)	2.096(3)	2.085(5)	2.149(8)	2.109(4)	1.968(6)
Fe(1)–N(3)	2.029(3)	2.038(7)	2.054(3)	2.0910(18)	2.081(11)	2.097(3)	2.099(4)	2.082(5)	2.125(4)	2.047(6)
Fe(1)–N(4)	2.016(3)	2.059(7)	2.047(3)	2.0218(18)	2.092(10)	2.079(3)	2.103(4)	2.100(5)	2.101(4)	1.990(7)
Fe(1)–O(1)/O(6)	2.157(2)	2.167(6)	1.923(3)	2.1435(15)	1.967(11)		1.984(3)			
Fe(1)–O(4)/N(5)					2.106(3)		1.994(5)	2.102(5)		
Fe(2)–N(5)				2.464(n.b.)		2.625(n.b.)			2.140(7)	
Fe(2)–N(6)				2.075(12)		2.124(4)			1.976(6)	
Fe(2)–N(7)				2.083(11)		2.079(5)			1.984(7)	
Fe(2)–N(8)				2.089(12)		2.116(4)			2.012(7)	
Fe(2)–O(2)/O(3)				1.981(10)		1.999(4)				
Fe(1)–[N(2), N(3), N(4)] ^a	0.3794	0.4795	0.0783 ^b	0.4120	0.6565	0.5251	0.6743	0.6573	0.6223	0.2764
Fe(2)–[N(6), N(7), N(8)] ^a					0.6517		0.7613			0.2422

^a Distance of Fe from mean plane. ^b Fe(1)–[O(1), N(3), N(4)]

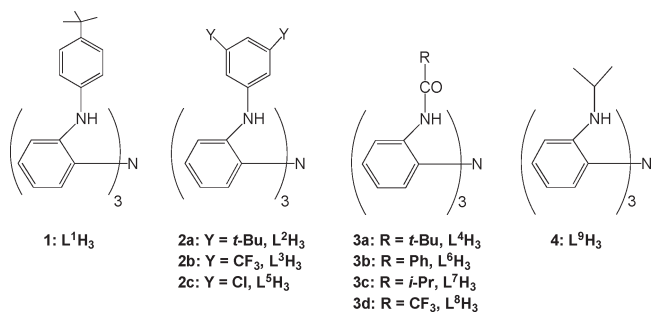
presented here. The structures of the precursor amine LH₃ and ligand L¹H₃ (**1**) have been previously reported.^{26a} The structures of ligands L²H₃ (**2a**), L⁴H₃ (**3a**), L⁶H₃ (**3b**, cocrystallized with PPh₄Cl), L⁷H₃ (**3c**), L⁸H₃ (**3d**), and L⁹H₃ (**4**) are shown in Figures S1–S6 (Supporting Information). Crystallographic data for these ligands are collected in Table S1 (Supporting Information). With the exception of L⁶H₃, which features a propeller-type structure that minimizes repulsion among the electron-rich

aryl groups, all other ligand structures exhibit a preorganized C₃-symmetric cavity (albeit distorted), which is predisposed to capture metal ions via a minimal trigonal pyramidal geometry after deprotonation of the ligand.

Synthesis of Fe(II) Complexes. The general methodology used for the preparation of the Fe(II) compounds calls for deprotonation of the tripodal ligands with 3 equiv of KH, followed by the addition of anhydrous FeCl₂ under an inert atmosphere. The reaction is usually

Table 3. Selected Angles (deg) for Compounds 6–15

	6	7	8	9	10	11	12	13	14	15
N(1)–Fe(1)–N(2)	77.23(11)	77.8(2)		76.91(7)		74.76(10)		72.4(3)	73.26(13)	83.1(3)
N(1)–Fe(1)–N(3)	80.00(11)	75.3(2)	79.77(11)	78.16(7)		75.89(10)		71.88(18)	72.90(13)	80.3(2)
N(1)–Fe(1)–N(4)	80.69(12)	76.8(2)	80.63(12)	80.39(7)		75.66(10)		71.44(17)	72.37(13)	82.6(3)
N(1)–Fe(1)–O(1)	168.44(10)	160.4(2)	102.19(11)	172.45(6)			177.89(10)		174.4(2)	178.05(15)
N(1)–Fe(1)–O(4)/N(5)										
N(2)–Fe(1)–N(3)	110.74(12)	106.6(3)		112.83(7)	104.0(4)	113.22(10)	112.06(17)	114.8(3)	115.93(14)	112.9(3)
N(2)–Fe(1)–N(4)	127.70(12)	105.0(3)		128.91(7)	125.0(4)	109.97(11)	108.01(17)	112.0(3)	110.70(14)	123.2(3)
N(3)–Fe(1)–N(4)	111.17(13)	131.6(3)	117.90(12)	106.24(7)	101.6(4)	118.49(11)	110.40(17)	105.5(2)	107.38(14)	118.2(3)
N(2)–Fe(1)–O(1)	96.65(11)	121.8(2)		97.98(7)						
N(3)–Fe(1)–O(1)	111.47(11)	96.5(3)	107.88(12)	109.12(6)						
N(4)–Fe(1)–O(1)	95.84(11)	96.9(2)	133.75(12)	98.99(7)						
N(2)–Fe(1)–O(1)/O(6)					112.6(4)		111.05(16)			
N(3)–Fe(1)–O(1)/O(6)					111.3(4)		104.43(16)			
N(4)–Fe(1)–O(1)/O(6)					101.8(4)		110.91(16)			
N(2)–Fe(1)–O(4)/N(5)						103.92(11)		105.1(3)	104.86(15)	
N(3)–Fe(1)–O(4)/N(5)						106.19(11)		113.7(2)	107.74(16)	
N(4)–Fe(1)–O(4)/N(5)						103.42(11)		105.5(2)	109.01(15)	
N(5)–Fe(2)–N(6)										83.3(3)
N(5)–Fe(2)–N(7)										83.4(3)
N(5)–Fe(2)–N(8)										82.3(3)
N(6)–Fe(2)–N(7)					105.8(5)		109.08(18)			122.5(3)
N(6)–Fe(2)–N(8)					105.0(5)		111.18(17)			115.1(3)
N(7)–Fe(2)–N(8)					120.8(4)		102.75(18)			117.9(3)
N(6)–Fe(2)–O(2)/O(3)					110.9(4)		107.89(17)			
N(7)–Fe(2)–O(2)/O(3)					111.6(4)		107.02(17)			
N(8)–Fe(2)–O(2)/O(3)					102.5(5)		118.48(16)			

Scheme 1

conducted in tetrahydrofuran (THF), but for ligands with more limited solubility, such as L^4H_3 , L^7H_3 , and L^8H_3 , dimethylacetamide (DMA) can be used instead. After the removal of insoluble KCl, isolation of the Fe(II) products is achieved largely by layering pentane over concentrated THF, or diethyl ether over DMA, which provides good yields of bulk material of high-purity for further exploration. Crystalline materials suitable for X-ray diffraction analysis usually require the slow diffusion of pentane into THF, or diethyl ether into DMA, at low temperatures.

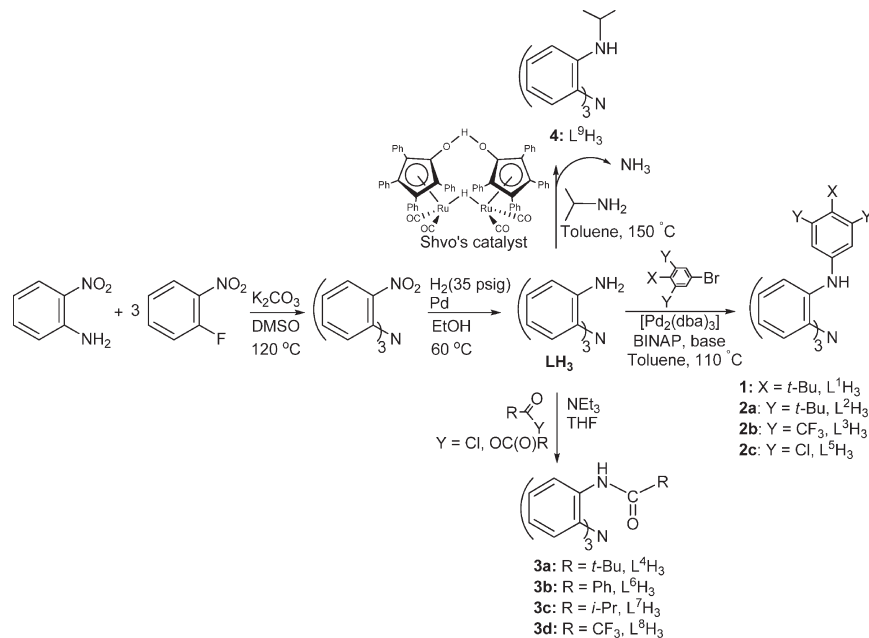
The coordination sphere of the ferrous site in the solid state can vary significantly (Scheme 3). On a number of occasions, the simple stoichiometry $[(L^x)\text{Fe(II)}-\text{THF}]^-$ ($L^x = L^1$ (**5**), L^2 (**6**), L^3 (**7**), L^5 (**9**)) or $[(L^x)\text{Fe(II)}-\text{DMA}]^-$ ($L^x = L^8$ (**13**)) is obtained. However, when acyl arms are involved, the carbonyl oxygen of the ligand, either of the same ferrous site or an adjacent one, can effectively compete for coordination at the expense of THF or DMA. This situation is encountered with ligands L^4 (**8**), L^6 (**10**), and L^7 (**12**), with the additional caveat that L^4 is O-atom-coordinated to Fe(II) in **8** via a $\text{N}(\text{Ar})=\text{C}(\text{R})-\text{O}^-$ residue rather than the more typical N-atom coordinated $\text{N}(\text{Ar})-\text{C}(\text{R})=\text{O}$ isomer. On the other hand, when acetonitrile is used for recrystallization, the

general stoichiometry $[(L^x)\text{Fe(II)}-\text{NCMe}]^-$ ($L^x = L^6$ (**11**), L^8 (**14**)) has always been obtained. Finally, the extreme case of $[\text{K}(L^9)\text{Fe(II)}]_2$ (**15**) is noted, in which the strong equatorial ligand field imposed by the arylalkylamido residues weakens the axial ligation and leads to a compound devoid of any solvent, coordinated or solvated. Also noteworthy is the contribution of the potassium counterion, which via association with electron-rich ligand moieties leads frequently to the generation of polymeric units in the solid state. Further details of the solid-state structures are provided below.

Solid-State Structures. $[(L^x)\text{Fe(II)}-\text{solv}]^-$ ($L^x = L^2$ (**6**), L^3 (**7**), L^5 (**9**), $\text{solv} = \text{THF}$; $L^x = L^8$ (**13**), $\text{solv} = \text{DMA}$; $L^x = L^6$ (**11**), L^8 (**14**), $\text{solv} = \text{MeCN}$). Structures that feature a solvent molecule coordinated to the Fe(II) site exhibit a trigonal bipyramidal (TBP) geometry, which is distorted to various degrees. $[(L^3)\text{Fe(II)}-\text{THF}]^-$ (**7**) proved to possess a structure (Figure 1) most deviating from TBP geometry, as exemplified by the $\text{N}(1)_{\text{amine}}-\text{Fe(1)}-\text{O}(1)_{\text{THF}}$ angle along the axial dimension, and a combination of two acute and one wide angle in the equatorial coordination plane. Moreover, the Fe(II) atom lies significantly off the equatorial plane of the three amido nitrogens, due to the structural requirements of the five-membered metalated rings (average $\text{N}_{\text{amine}}-\text{Fe(1)}-\text{N}_{\text{amido}} = 76.6(2)^\circ$). The structures of $[(L^2)\text{Fe(II)}-\text{THF}]^-$ (**6**), $[(L^5)\text{Fe(II)}-\text{THF}]^-$ (**9**) (Figure 1), and $[(L^1)\text{Fe(II)}-\text{THF}]^-$ (**5**)^{26b} are by comparison less distorted, especially along the axial coordination, while the angle distortion in the equatorial plane and the deviation of the Fe(II) atom from the mean plane of the three N_{amido} atoms remain pronounced. The role of K^+ as a structural element will be detailed in a subsequent section.

The structure of $[(L^8)\text{Fe(II)}-\text{DMA}]^-$ (**13**) (Figure 2) is more distorted from the C_3 symmetry, whereas the corresponding acetonitrile adducts $[(L^8)\text{Fe(II)}-\text{NCMe}]^-$ (**14**) and $[(L^6)\text{Fe(II)}-\text{NCMe}]^-$ (**11**) (Figure 2) are the least

Scheme 2



perturbed *C*₃-symmetric structures noted in this study. Nevertheless, the significantly longer Fe(1)–N(2) bond in [(L⁸)Fe(II)–DMA][–] (Figure 2) is accompanied by a short N(2)–C(7) (1.168(12) Å) and a long C(7)–O(1) (1.336(12) Å) bond, suggesting –O–C(CF₃)=(Ar)N–Fe coordination. The metrical parameters associated with the other two N_{amide} residues, as well as those observed for all three N_{amide} units of [(L⁸)Fe(II)–NCMe][–], are consistent with O=C(CF₃)–(Ar)N–Fe coordination. The deviation of the Fe(II) atom from the mean plane defined by the three N_{amide} atoms is very significant for all three compounds.

The average Fe–N_{amide} bond distances (2.030 (L¹), 2.036 (L²), 2.049 (L³), 2.065 (L⁵), 2.091 (L⁶), and 2.111 Å (L⁸)) reflect the strength of the equatorial ligand field in accordance with the electron-donating capabilities of the ligands noted above. However, deviations from the average Fe–N_{amide} bond distances are significant and can be attributed to the presence of K⁺ ions that make close contacts with aromatic and other electron-rich residues associated with specific N_{amide} atoms, leading to elongation of the corresponding Fe–N_{amide} bond distance. For instance, the presence of a K⁺–(η⁶-arene) interaction involving the phenylene group between atoms N(4) and N(1) in [(L³)Fe(II)–THF][–] (7, Figure 1) is responsible for the longer Fe(1)–N(4) bond in this compound.

The presence of K⁺ ions is also responsible for tertiary structures observed in the packing of the unit cell. Whereas [K(THF)₃][(L¹)Fe(II)–THF]·0.5THF (5)^{26b} and [K(THF)₃][(L²)Fe(II)–THF] (6) are strictly monomeric, [K(THF)₂][(L³)Fe(II)–THF] adopts a centrosymmetric dimeric structure by virtue of mutual close contacts between the K⁺ ion of each molecule and a fluorine atom of the partner molecule (K–FCF₂Ar = 2.735 Å, Figure 1). In contrast, [K(L⁵)Fe(II)–THF] (9) exhibits an array of K⁺ ions connecting ligand residues of adjacent molecules, giving rise to a one-dimensional polymeric structure. Furthermore, [K(NCMe)][(L⁶)Fe(II)–NCMe]·2MeCN (11), [K(NCMe)][(L⁸)Fe(II)–NCMe]

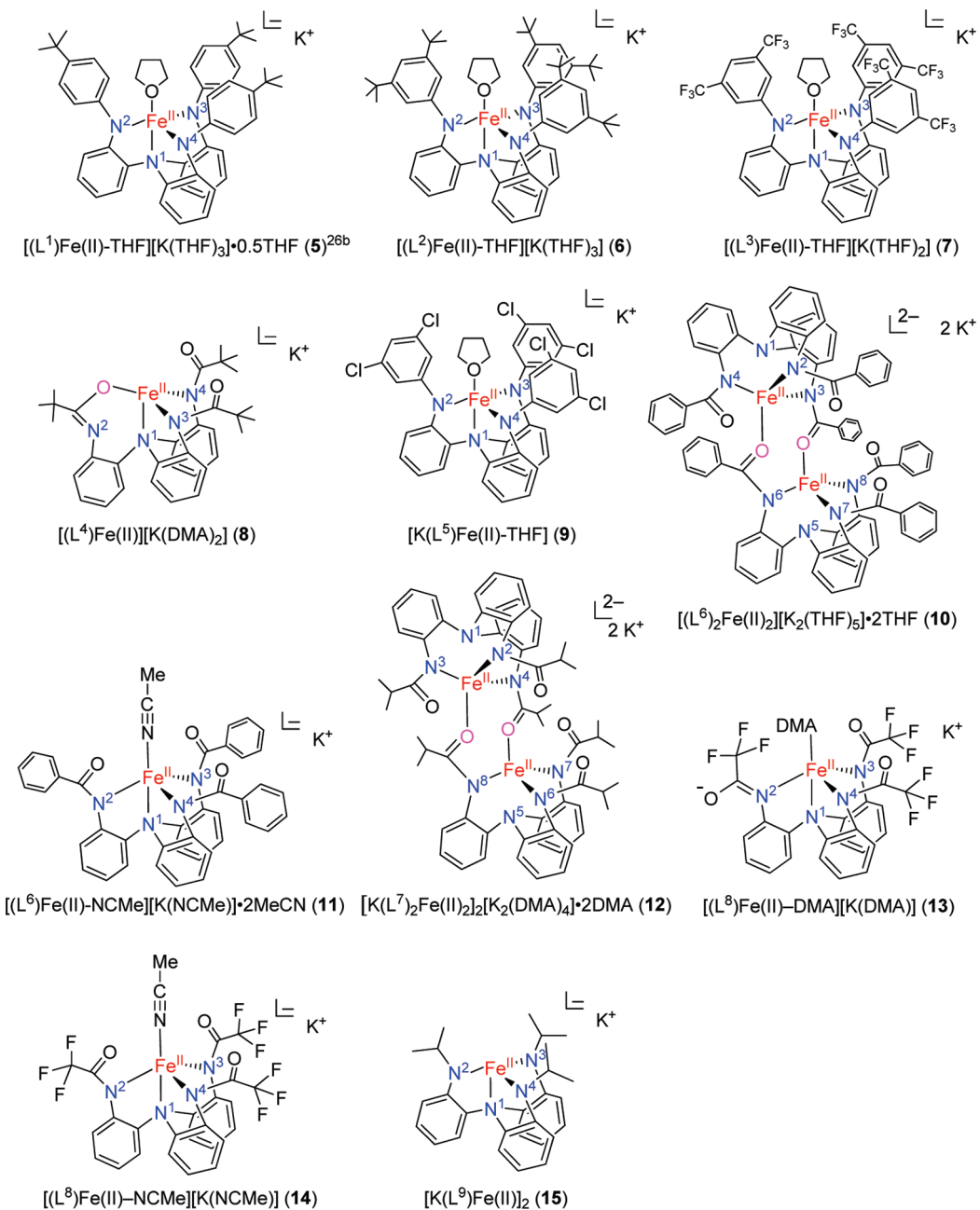
(14), and [K(DMA)][(L⁸)Fe(II)–DMA] (13) demonstrate the same potassium-induced, three-dimensional architecture, featuring K(solv)⁺ ions that are coordinated by all three amidato carbonyl moieties (O(1), O(2), and O(3)), each belonging to a different molecule (best shown for [K(NCMe)][(L⁸)Fe(II)–NCMe] (14) in Figure 2).

Structures of [(L⁴)Fe(II)][K(DMA)]₂ (8), [K₂(THF)₅][(L⁶)₂Fe(II)₂]·2THF (10), and [K₂(DMA)₄][K(L⁷)₂Fe(II)₂]₂·2DMA (12). The common characteristic of these structures is the absence of a metal-coordinating solvent molecule, and its replacement by an amidato residue³⁷ through the carbonyl oxygen atom. The structure of [K(DMA)₂][(L⁴)Fe(II)] (8) (Figure 3) is the simplest of all three, but also unique, inasmuch as one of the equatorial N_{amide} atoms remains outside the coordination sphere (Fe(1)···N(2) = 3.350 Å), while the corresponding amidato oxygen atom is preferentially bonded to the four-coordinate metal site via the (Ar)N=C(*t*-Bu)–O[–] coordination mode. The Fe(II) site deviates only slightly from the [O(1), N(3), N(4)] mean plane. The structure is in reality polymeric, because each DMA-solvated K⁺ ion is also associated with carbonyl atoms O(2) and O(3) belonging to adjacent molecules.

The structure of [K₂(THF)₅][(L⁶)₂Fe(II)₂]·2THF (10) (Figure 4) features a slightly asymmetric dimer with two ferrous sites differing in their metrical parameters by a small margin (average Fe(1)–N_{amide} = 2.085 Å; Fe(2)–N_{amide} = 2.082 Å). The coordination sphere of each Fe(II) is essentially similar to that of the trigonal bipyramidal [K(NCMe)][(L⁶)Fe(II)–NCMe]·2MeCN (11) (Figure 2), save for two major modifications: (a) the axial N_{amine} atoms make very weak contacts, if at all, with the metal sites, and (b) the axial coordination sites trans to those N_{amine} atoms are occupied by carbonyl moieties provided by an amidato residue of the partner monomer. The metrical parameters associated with the amidato

(37) Leitch, D. C.; Beard, J. D.; Thomson, R. K.; Wright, V. A.; Patrick, B. O.; Schafer, L. L. *Eur. J. Inorg. Chem.* **2009**, 2691–2701.

Scheme 3



units are consistent with an $\text{Fe}(1,2)-\text{N}(\text{Ar})-\text{C}(\text{Ph})=\text{O}-\text{Fe}(2,1)$ coordination mode. The mutual amidato contacts are responsible for holding the dimer together, further assisted by both K^+ counterions, each coordinated, at least, by an amidato carbonyl moiety from each ligand, and also by one ($\text{K}(1)$) and four ($\text{K}(2)$) THF molecules, respectively (Figure 5). These solvent molecules are responsible for terminating the dimeric molecular entity and not allowing any dimer–dimer interactions via K^+ bridging.

The structure of $[\text{K}_2(\text{DMA})_4][\text{K}(L^7)_2\text{Fe}(\text{II})_2] \cdot 2\text{DMA}$ (12) (Figure 4) is the most complicated of all, featuring a dimer of dimers within an overall polymeric construct. The individual dimer is not unlike the one discussed with regard to the structure of $[\text{K}_2(\text{THF})_5][(L^6)_2\text{Fe}(\text{II})_2] \cdot 2\text{THF}$ (10); it is similarly asymmetric (average $\text{Fe}(1)-$

$\text{N}_{\text{amide}} = 2.096 \text{ \AA}$; $\text{Fe}(2)-\text{N}_{\text{amide}} = 2.106 \text{ \AA}$), the N_{amide} atoms are essentially noncoordinated, and the axial coordination is provided by the amidato carbonyl molecule of the partner ligand.

The $\text{Fe}(1)/\text{Fe}(2)$ and $\text{Fe}(3)/\text{Fe}(4)$ dimers of the repeating unit ($[\text{Fe}(1)/\text{Fe}(2) \cdots \text{K}(1)-\text{O}(10) \cdots \text{Fe}(3)/\text{Fe}(4) \cdots \text{K}(2)-\text{O}(1)]$) differ slightly in their metrical parameters (average $\text{Fe}(3)-\text{N}_{\text{amide}} = 2.097 \text{ \AA}$; $\text{Fe}(4)-\text{N}_{\text{amide}} = 2.099 \text{ \AA}$) and are interconnected via one of their respective K^+ ions ($\text{K}(1)$ or $\text{K}(2)$; Figure 5). Each of these K^+ ions is attached to carbonyl residues and other electron-rich entities of one dimer, and to a unique amidato carbonyl residue of the second dimer ($\text{K}(1)-\text{O}(10)$ and $\text{K}(2)-\text{O}(1)$). The N -atom ends of these unique amidato residues, $\text{N}(14)$ and $\text{N}(2)$, are connected to atoms $\text{Fe}(1)$ and $\text{Fe}(4)$, respectively. These K^+ ions are also very similar in

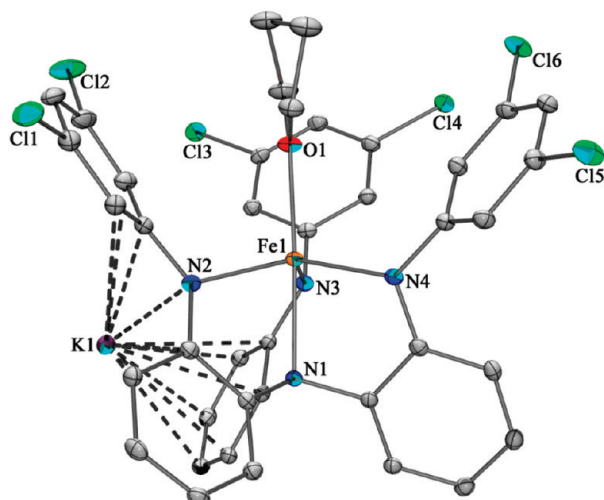
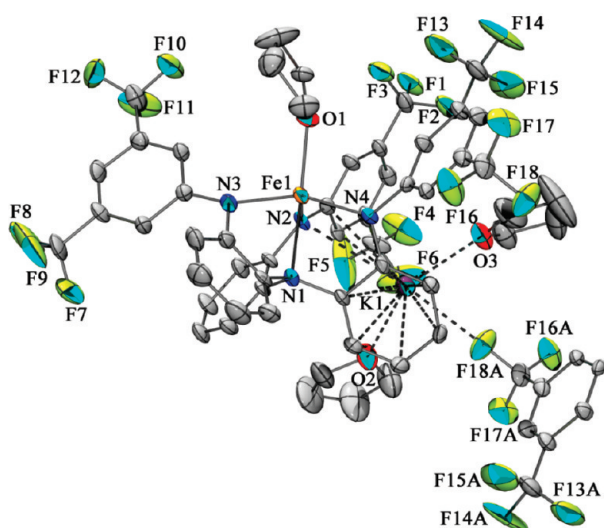
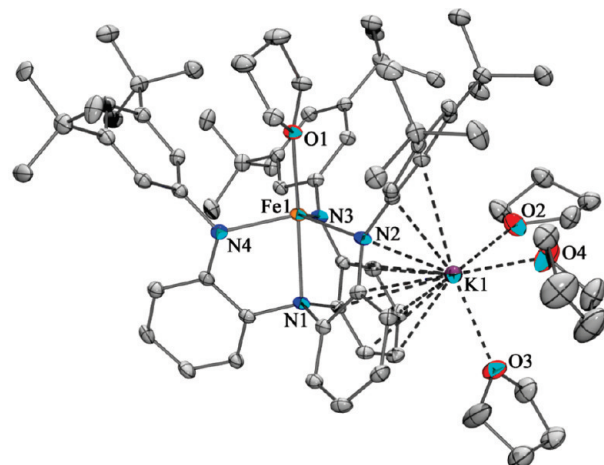


Figure 1. Solid-state structures of $[K(\text{THF})_3][(\text{L}^2)\text{Fe(II)}-\text{THF}]$ (**6**, top), $[K(\text{THF})_2][(\text{L}^3)\text{Fe(II)}-\text{THF}]$ (**7**, middle), and $[K(\text{L}^5)\text{Fe(II)}-\text{THF}]$ (**9**, bottom), showing 30% probability ellipsoids and the atom labeling scheme. $K \cdots F$ interaction between adjacent molecules is also shown for **7**.

coordination to that of the K(1) ion of $[K_2(\text{THF})_5][(\text{L}^6)_2\text{Fe(II)}_2 \cdot 2\text{THF}]$ (**10**) that carries the single THF molecule, with the exception that the THF molecule is here replaced by the unique amidato moiety. However, the present

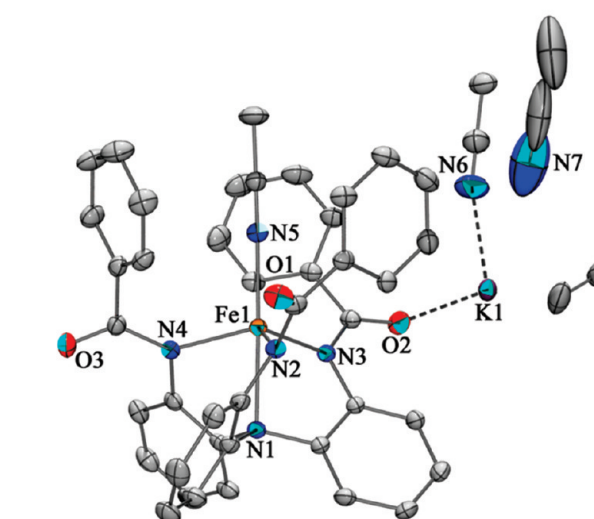
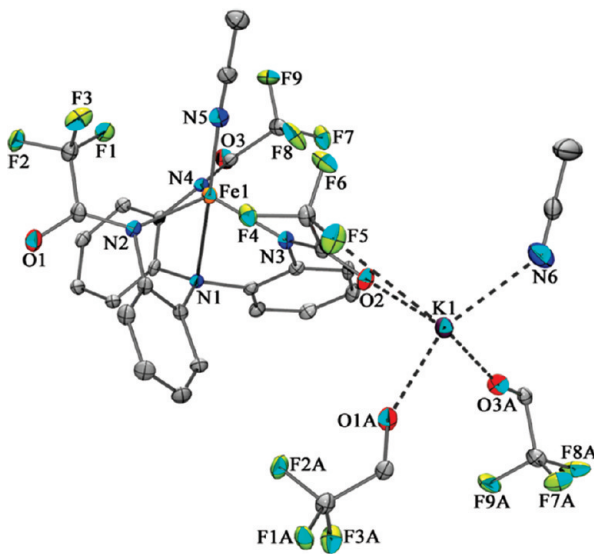
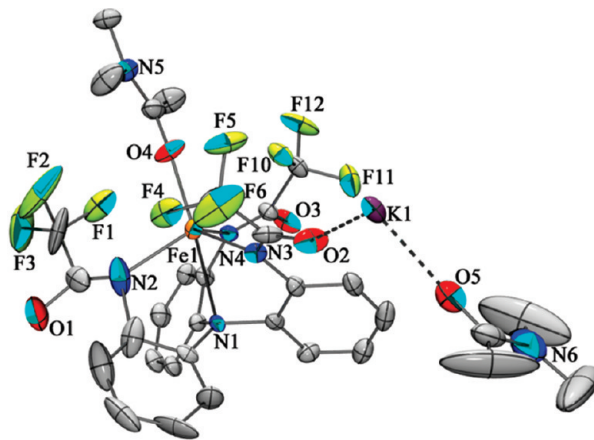


Figure 2. Solid-state structures of $[K(\text{DMA})][(\text{L}^8)\text{Fe(II)}-\text{DMA}]$ (**13**, top), $[K(\text{NCMe})][(\text{L}^8)\text{Fe(II)}-\text{NCMe}]$ (**14**, middle), and $[K(\text{NCMe})][(\text{L}^8)\text{Fe(II)}-\text{NCMe}] \cdot 2\text{MeCN}$ (**11**, bottom), showing 30% probability ellipsoids and the atom labeling scheme.

K^+ -induced, three-dimensional structure is more complicated, because the remaining two K^+ ions ($K(3)$ and $K(4)$) form an interesting $[K_2(\text{DMA})_4]$ dimer, composed of two bridging DMA molecules and two terminal DMA

molecules attached to K(4). The coordination is completed by a bridging atom (O(7)) of an amidato carbonyl moiety belonging to the Fe(3)/Fe(4) dimer, and a terminal atom (O(4)) of an amidato carbonyl residue belonging to

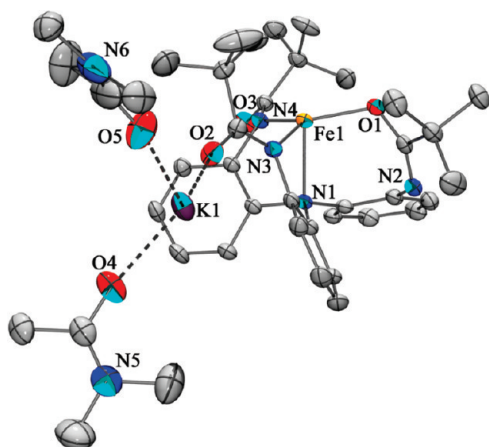


Figure 3. Solid-state structure of $[K(DMA)_2][L^4Fe(II)]$ (**8**), showing 30% probability ellipsoids and the atom labeling scheme.

the Fe(1)/Fe(2) dimer. The *N*-atom ends (N(10) and N(6)) of these two amidato residues are attached to atoms Fe(3) and Fe(2), respectively. The overall architecture is thus one in which the pseudo 1-D polymer with the repeating $[Fe(1)/Fe(2)\cdots K(1)\cdots Fe(3)/Fe(4)\cdots K(2)]$ motif is linked to identical 1-D arrays via lateral connections provided by the K(3)/K(4) dimers.

Structure of $[K(L^9)Fe(II)]_2$ (15**).** The tripodal arylalkylamido-amine ligand L⁹ affords a ferrous compound, whose structure is unique. Although crystallized from THF/pentane, the compound is devoid of any solvent residue in the unit cell. Two ferrous sites are observed as being interconnected by means of K⁺ contacts to electron-rich moieties of adjacent $[(L^9)Fe(II)]$ units to generate an $-[Fe(1)-K(1)-Fe(2)-K(2)]_n-$ sequence (Figure 6). More specifically, K(1) is shown to be involved in K⁺-(η^6 -arene) interactions between adjacent phenylene moieties, as well as in long-range contacts with N(4) and C(20) (K(1)-N(4)=3.127(7), K(1)-C(20)=3.535(8) Å). Similarly, K(2) is engaged in K⁺-(η^6 -arene) contacts (phenylene rings between N(5)/N(8) and N(1)/N(2)) and in long-range interactions with atoms N(3), N(7), and C(37) (K(2)-N(3)=3.089(7), K(2)-N(7)=3.067(7), and

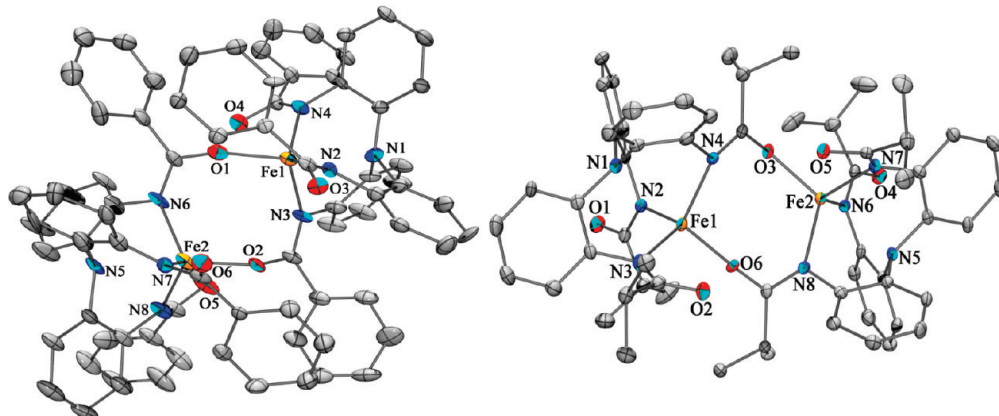


Figure 4. Solid-state structures of the anions of $[K_2(THF)_5][(L^6)_2Fe(II)_2] \cdot 2THF$ (**10**, left) and $[K_2(DMA)_4][K(L^7)_2Fe(II)_2]_2 \cdot 2DMA$ (**12**, right; only one dimer shown), showing 30% probability ellipsoids and the atom labeling scheme.

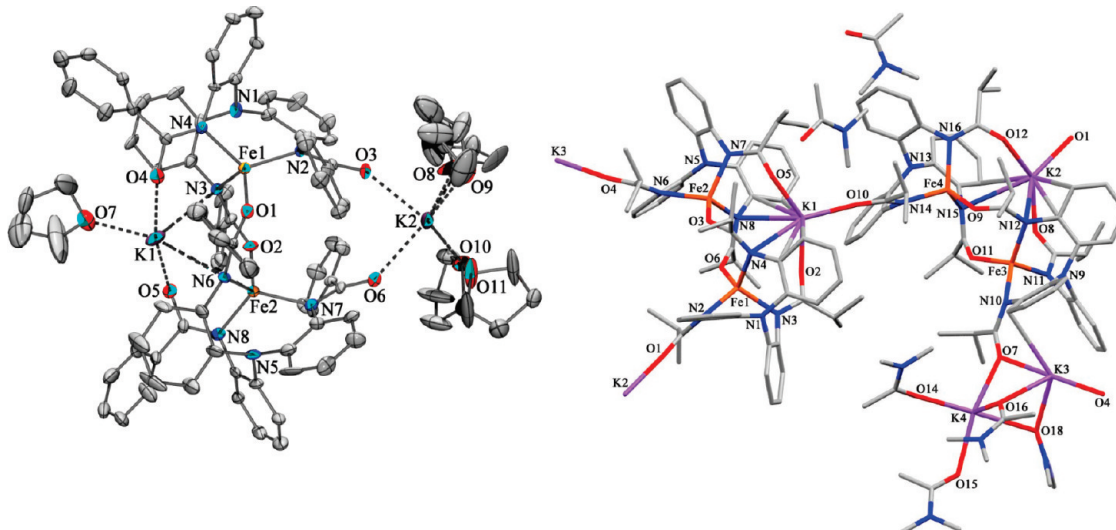


Figure 5. Solid-state structures of $[K_2(THF)_5][(L^6)_2Fe(II)_2] \cdot 2THF$ (**10**, left) and $[K_2(DMA)_4][K(L^7)_2Fe(II)_2]_2 \cdot 2DMA$ (**12**, right), showing the respective positions of the K⁺ ions with regard to the diferrous units.

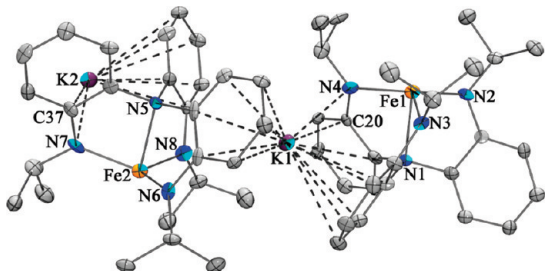


Figure 6. Solid-state structure of $[K(L^9)Fe(II)_2]$ (**15**), showing 30% probability ellipsoids and the atom labeling scheme.

$K(2)-C(37) = 3.425(7)$ Å. However, these contacts are arbitrarily allowed by means of the rather generous upper limits set by the sum of Bondi's intermolecular van der Waals radii (K, 2.75; C, 1.70; and K, 1.55 Å),³⁸ and not all of them can be considered as genuine interactions. In particular, the long-distance K^+ contacts to C(20) and C(37) are doubtful. The two ferrous sites differ slightly in their metrical parameters and feature a tight four-coordinate ligand field generated by the electron-rich arylalkylamido residues (average $Fe(1)-N_{\text{amide}} = 2.002$ Å; $Fe(2)-N_{\text{amide}} = 1.991$ Å) and the apical N_{amine} atom. As expected, the strong trigonal-pyramidal ligand field weakens considerably the axial coordination trans to the N_{amine} atom, which remains free of any solvent. In acetonitrile solutions, compound **15** readily releases the ligand L^9H_3 via an unidentified pathway.

It has not been possible to ascertain whether the structures of compounds **6–15** are retained in solution. Efforts to obtain ESI-MS data have been hampered by the sensitivity of these compounds to oxidative events. NMR data provided in the Experimental Section suggest that the low symmetry observed in the solid state (absence of a strict C_3 axis in all structures) is reflected in fluid matrices, but the situation is further complicated due to the uncertainty regarding the coordination of the potassium ions in different solvents. Therefore, the NMR data reported should be treated as markers for identification purposes and not necessarily as true representatives of the solid structures.

Mössbauer Spectroscopy. Zero-field Mössbauer spectra from powdered samples were recorded at liquid nitrogen temperatures. Parameters are shown in Table 4. Representative spectra are shown in Figure 7. The remaining spectra are shown in Figures S7–S12 (Supporting Information). For mononuclear complexes $[(L^x)Fe(II)-\text{solv}]^-$ ($L^x = L^1$ (**5**), L^2 (**6**), L^3 (**7**), L^5 (**9**), solv = THF; L^8 , solv = DMA (**13**), MeCN (**14**) as well as $[K(DMA)_2][(L^4)Fe(II)]$ (**8**), the spectra consist of a unique quadrupole doublet. For complexes $[K_2(\text{THF})_5][(L^6)_2Fe(II)_2 \cdot 2\text{THF}]$ (**10**), $[K_2(\text{DMA})_4][K(L^7)_2Fe(II)_2 \cdot 2\text{DMA}]$ (**12**), and $[K(L^9)Fe(II)]_2$ (**15**), the spectra are more complicated, in agreement with the structural data.

In all cases, the Mössbauer parameters, and especially the isomer shifts (ranging from 0.75 to 1.14 mm/s), are

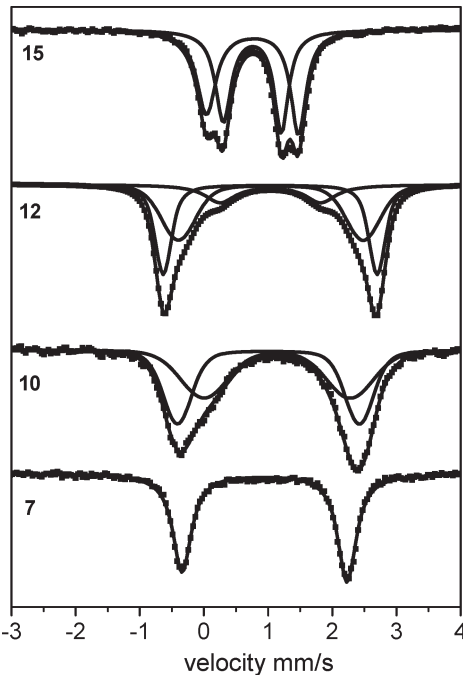


Figure 7. The 78 K Mössbauer spectra from powdered samples of compounds $[K(\text{THF})_2]_2[(L^3)\text{Fe(II)}-\text{THF}]$ (**7**), $[K_2(\text{THF})_5]_2[(L^6)_2\text{Fe(II)}] \cdot 2\text{THF}$ (**10**), $[K_2(\text{DMA})_4][K(L^7)_2\text{Fe(II)}_2]_2 \cdot 2\text{DMA}$ (**12**), and $[K(L^9)\text{Fe(II)}]_2$ (**15**), as indicated. Solid lines are theoretical simulations as described in the text.

indicative of high-spin Fe(II) ($S = 2$) species³⁹ in a N/O ligand environment.⁴⁰ For all ferrous complexes that feature a solvent molecule in the coordination sphere (**5–7**, **9**, **13**, and **14**), the value for the isomer shift⁴¹ is consistent with that reported for other five-coordinate ferrous sites⁴² and is narrowly distributed around 1.0 mm/s. Compound **13** has the highest isomer shift value in this series, since, by comparison to **14**, it possesses a weaker ligand field, owing to the imino N -atom residue and the coordinated DMA.

The variation of the quadrupole splitting for the ferrous sites is noteworthy, but with the exception of the ΔE_Q values for **15** (see below), the range is much narrower, in agreement with the values reported for the vast majority of high-spin Fe(II) ($S = 2$) complexes ($\Delta E_Q = 2.5–3.5$ mm/s).⁴³ The variation of the quadrupole splitting for the solvated ferrous sites reflects small differences in the coordination environment, especially local stereochemical twists that induce asymmetry, which cannot be fully accounted for at the present stage of the investigation.

For dimeric compound **10**, the existence of two different doublets is in agreement with the slightly different geometric characteristics of the two ferrous sites. For **12**, which is structurally a dimer of dimers, only two doublets

(38) (a) Bondi, A. *J. Phys. Chem.* **1964**, *68*, 441–451. (b) Rowland, R. S.; Taylor, R. *J. Phys. Chem.* **1996**, *100*, 7384–7391. (c) Mantina, M.; Chamberlin, A. C.; Valero, R.; Cramer, C. J.; Truhlar, D. G. *J. Phys. Chem. A* **2009**, *113*, 5806–5812.

(39) Müncck, E. *Physical Methods in Inorganic and Bioinorganic Chemistry*; University Science Books: Sausalito, CA, 2000; Chapter 6, pp 287–319.

(40) (a) Weber, B.; Kaps, E. S.; Desplanches, C.; Létard, J.-F.; Achterhold, K.; Parak, F. G. *Eur. J. Inorg. Chem.* **2008**, 4891–4898. (b) Weber, B.; Carbonera, C.; Desplanches, C.; Létard, J.-F. *Eur. J. Inorg. Chem.* **2008**, 1589–1598.

(41) Andres, H.; Bominaar, E. L.; Smith, J. M.; Eckert, N. A.; Holland, P. L.; Müncck, E. *J. Am. Chem. Soc.* **2002**, *124*, 3012–3025.

(42) (a) Hu, C.; Noll, B. C.; Schulz, C. E.; Scheidt, W. R. *Inorg. Chem.* **2008**, *47*, 8884–8895. (b) Hachem, I.; Belkhiria, M. S.; Giorgi, M.; Schulz, C. E.; Nasri, H. *Polyhedron* **2009**, *28*, 954–958.

(43) Kurtz, D. M., Jr. *Chem. Rev.* **1990**, *90*, 585–606.

Table 4. Mössbauer Parameters at 78 K and Electrochemical Data at Room Temperature for Compounds 5–15

	δ (mm/s)	ΔE_Q (mm/s)	Area (%)	$E_{1/2}$ (or $E_{p,a}$) (V vs Fc^+/Fc)	ΔE (mV)	$i_{p,a}/i_{p,c}$
[K(THF) ₃][$(\text{L}^1)\text{Fe}(\text{II})-\text{THF}$]·0.5THF (5) ^{26a}	0.96	2.60	100	-1.302 (DMSO) ^{26a} -1.298 (DMF) ^{26a}	81 71	1.23 1.16
[K(THF) ₃][$(\text{L}^2)\text{Fe}(\text{II})-\text{THF}$] (6)	0.96	3.16	100	-1.326 (DMSO) -1.348 (DMF)	88 71	1.05 1.09
[K(THF) ₂][$(\text{L}^3)\text{Fe}(\text{II})-\text{THF}$] (7)	0.95	2.57	100	-0.791 (DMSO)	92	1.14
[K(DMA) ₂][$(\text{L}^4)\text{Fe}(\text{II})$] (8)	0.96	2.86	100	-0.640 (DMF)		
[K(L^5)Fe(II)-THF] (9)	0.96	2.60	100	-0.841 (DMSO) -0.859 (DMF)	72 70	1.15 1.53
[K ₂ (THF) ₅][$(\text{L}^6)\text{Fe}(\text{II})_2 \cdot 2\text{THF}$] (10)	site 1 site 2	1.00 1.14	2.83 2.28	50 50	-0.567 (DMSO) -0.93, -0.76, -0.534 (THF) -0.572 (DMSO)	69 56
[K(NCMe)][$(\text{L}^6)\text{Fe}(\text{II})-\text{NCMe}$]·2MeCN (11)	site 1 site 2 site 3	1.04 1.04 1.01	3.34 2.97 1.69	37 49 12	-0.904, -0.720 (DMA) -0.705 (DMSO) -1.19, -0.92, -0.684 (DMF)	73, 72
[K(DMA)][$(\text{L}^8)\text{Fe}(\text{II})-\text{DMA}$] (13)		1.12	3.34	100	0.013 (DMA)	
[K(NCMe)][$(\text{L}^8)\text{Fe}(\text{II})-\text{NCMe}$] (14)		1.04	2.98	100	0.140 (MeCN) 0.017 (DMF)	165 2.54
[K(L^9)Fe(II)] ₂ (15)	site 1 site 2	0.75 0.76	0.91 1.43	47 53	-1.185, -0.913 (DMF)	

could be safely discerned and simulated, without taking the risk of overparametrization. Apparently, the two dimers in **12** are indistinguishable by Mössbauer spectroscopy. It should also be noted that an unidentified ferrous site, which accounts for approximately 12% of the signal area and exhibits a significantly different ΔE_Q , has been encountered in all analytically pure samples of **12** tested. It is currently unknown if this minority site is due to a different phase that is not represented by the structure of **12**. The four Fe(II) ($S = 2$) sites are magnetically isolated at room temperature, as judged by a $\chi_M T$ value of 11.2 emu K mol⁻¹, measured on an Evans magnetic balance.

For complex **15**, the two ferrous sites exhibit the smallest isomer shift and quadrupole splitting values in the series. The isomer shift values are in agreement with the very strong ligand field in **15** and within the range expected for four-coordinate Fe(II) species,⁴⁴ as well as comparable with the isomer shift of [FeS₄]⁶⁻ moieties encountered in proteins such as reduced Rubredoxin⁴⁵ and synthetic analogs.⁴⁶ On the other hand, the ferrous sites in **15** exhibit substantially smaller ΔE_Q values, outside the typical range for ferrous sites. Nevertheless, a small but significant number of ferrous compounds with similarly low ΔE_Q values (and analogous δ values) have been discussed by Münck and co-workers⁴¹ in association with planar three-coordinate [$(\beta$ -diketiminate)Fe(II)(X)] species. The reader is referred to Münck et al.'s paper for further discussion of the ligand contributions,

(44) (a) Cowley, R. E.; Elhaik, J.; Eckert, N. A.; Brennessel, W. W.; Bill, E.; Holland, P. L. *J. Am. Chem. Soc.* **2008**, *130*, 6074–6075. (b) Cowley, R. E.; Bill, E.; Neese, F.; Brennessel, W. W.; Holland, P. L. *Inorg. Chem.* **2009**, *48*, 4828–4836. (c) Stoian, S. A.; Smith, J. M.; Holland, P. L.; Münck, E.; Bominar, E. L. *Inorg. Chem.* **2008**, *47*, 8687–8695. (d) Khusniyarov, M. M.; Weyhermüller, T.; Bill, E.; Wieghardt, K. *J. Am. Chem. Soc.* **2009**, *131*, 1208–1221. (e) Lu, C. C.; Bill, E.; Weyhermüller, T.; Bothe, E.; Wieghardt, K. *J. Am. Chem. Soc.* **2008**, *130*, 3181–3197. (f) Muresan, N.; Lu, C. C.; Ghosh, M.; Peters, J. C.; Abe, M.; Henling, L. M.; Weyhermüller, T.; Bill, E.; Wieghardt, K. *Inorg. Chem.* **2008**, *47*, 4579–4590.

(45) Debrunner, P. G.; Münck, E.; Que, L.; Schultz, C. E. *Iron Sulfur Proteins*; Lovenberg, W., Ed; Academic Press: New York, 1977; Vol. III, Chapter 10 and refs therein.

(46) (a) Lane, R. W.; Ibers, J. A.; Frankel, R. B.; Papaefthymiou, G. C.; Holm, R. H. *J. Am. Chem. Soc.* **1977**, *99*, 84–98. (b) Coucouvanis, D.; Swenson, D.; Baenziger, N. C.; Murphy, C.; Holah, D. G.; Sfarnas, N.; Simopoulos, A.; Kostikas, A. *J. Am. Chem. Soc.* **1981**, *103*, 3350–3362.

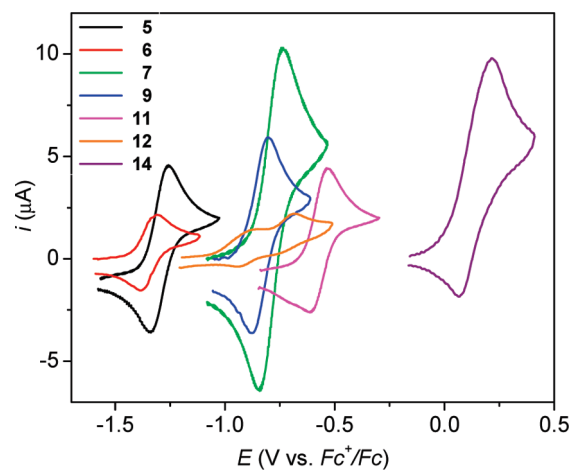


Figure 8. Cyclic voltammograms (Fe(II)/Fe(III)) of compounds [K(THF)₃][$(\text{L}^1)\text{Fe}(\text{II})-\text{THF}$]·0.5THF (**5**) and [K(THF)₃][$(\text{L}^2)\text{Fe}(\text{II})-\text{THF}$] (**6**), [K(THF)₂][$(\text{L}^3)\text{Fe}(\text{II})-\text{THF}$] (**7**), [K(L^5)Fe(II)-THF] (**9**) and [K(NCMe)][$(\text{L}^6)\text{Fe}(\text{II})-\text{NCMe}$]·2MeCN (**11**), in DMSO/[$(n\text{-Bu})_4\text{N}$]PF₆, [K₂(DMA)₄][$(\text{L}^7)\text{Fe}(\text{II})_2 \cdot 2\text{DMA}$] (**12**) in DMA/[$(n\text{-Bu})_4\text{N}$]PF₆, and [K(NCMe)][$(\text{L}^8)\text{Fe}(\text{II})-\text{NCMe}$] (**14**) in MeCN/[$(n\text{-Bu})_4\text{N}$]PF₆, as indicated, with a Au disk electrode (1.6 mm in diameter); scan rate, 0.1 V/s. Differences in current are due, in part, to differences in concentration (1.0–3.0 mM).

apparently both positive and negative, to the electric field gradient.

Electrochemistry. Electrochemical data are collected in Table 4. Cyclic voltammetry experiments on [$(\text{L}^1)\text{Fe}(\text{II})-\text{solv}$]⁻ (solv = THF (**5**),^{26b} DMF,^{26a} and DMSO^{26a}) under anaerobic conditions have previously provided a semireversible Fe(II)/Fe(III) couple at very negative potentials (Figure 8 and Figure S13, Supporting Information). The structurally and electronically related [$(\text{L}^2)\text{Fe}(\text{II})-\text{THF}$]⁻ (**6**) also furnishes a similar semireversible wave (Figure 8 and Figure S14, Supporting Information) at even more negative potentials, as expected due to the strong electron-donating character of the ligand. In DMSO, the wave has been obtained cathodically, after stoichiometric oxidation of Fe(II) to Fe(III), due to the extreme sensitivity of **6** to oxidation in DMSO. As expected, the related [$(\text{L}^3)\text{Fe}(\text{II})-\text{THF}$]⁻ (**7**) and [$(\text{L}^5)\text{Fe}(\text{II})-\text{THF}$]⁻ (**9**) in DMSO and DMF, which bear the electron-withdrawing aryl substituents 3,5-(CF₃)₂ and

3,5-Cl₂, respectively, exhibit a substantial anodic shift of their Fe(II)/Fe(III) redox couple (Figure 8 and Figures S15 and S17, Supporting Information) and are in agreement with the expected electronic character of these substituents.

The acyl-substituted ligands further accentuate the anodic shift of the Fe(II)/Fe(III) potential, as best illustrated by $[(L^6)Fe(II)-NCMe]^-$ (**11**), which demonstrates an almost reversible Fe(II)/Fe(III) wave in DMSO (Figure 8 and Figure S18, Supporting Information). The dimeric version of this compound, $[(L^6)_2Fe(II)]^{2-}$ (**10**), exhibits an almost identical cyclic voltammogram, suggesting that both compounds are monomeric in DMSO. The dimer **10** is crystallized in THF, and the cyclic voltammogram in this solvent only shows broad irreversible features (Figure S19, Supporting Information). In contrast, the structurally related $[K(L^7)_2Fe(II)]^{2-}$ (**12**) exhibits two closely spaced waves with narrow ΔE values in DMA (Figure 8 and Figure S20, Supporting Information), presumably due to the presence of the dimeric iron unit, whereas only irreversible features are observed in both DMSO and DMF (Figures S21 and S22, Supporting Information). Similarly, the structurally unique $[K(DMA)_2][(L^4)Fe(II)]$ (**8**) affords only a broad irreversible feature (Figure S16, Supporting Information). The strongly electron-withdrawing COCF₃ substituent of $[K(DMA)][(L^8)Fe(II)-DMA]$ (**13**) and $[K(NCMe)][(L^8)Fe(II)-NCMe]$ (**14**) furnishes an irreversible anodic wave for **13** in DMA (Figure S23, Supporting Information; coupled to three cathodic waves at $E_{p,c} = -0.116, -0.625$, and -1.083 V) and an anodic/cathodic wave for **14** in MeCN (Figure 8 and Figure S24, Supporting Information) or DMF (Figure S25, Supporting Information; coupled to two cathodic waves at $E_{p,c} = -0.114, -0.614$ V) shifted to much more positive potential values. Accordingly, compound **14** proved to be the most difficult to oxidize. Finally, the unique, alkyl-substituted $[K(L^9)Fe(II)]_2$ (**15**) shows two broad irreversible anodic waves (Figure S26, Supporting Information), which denote substantial stabilization of the ferric state as expected due to the electron-rich nature of the arylalkylamido-amine ligand, and may also reflect the presence of two slightly distinct iron sites. The irreversible character of the waves noted in this section makes the assignment of the Fe(II)/Fe(III) potential tentative (albeit reasonable with respect to the electronic character of each ligand) and cannot presently exclude contributions from ligand-centered events.

Conclusions

The following are the salient observations and findings of this work:

- (a) A family of *C*₃-symmetric triphenylamido-amine ligands, possessing a rigid tris(2-NH-phenyl)-amine core and a selection of aryl, acyl, and alkyl

arms has been synthesized and utilized in the synthesis of the corresponding ferrous complexes.

(b) In spite of the unique ligand framework, a multitude of structures are obtained for the synthesized Fe(II) complexes. Although the general stoichiometry $[LFe(II)-solv]^-$ (solv = THF, DMA, and MeCN) is encountered in many instances, significant distortions of the coordination sphere are apparent, with one extreme case indicating imino ($Fe-N(Ar)=C(R)-O^-$) rather than amido ($Fe-N(Ar)-C(R)=O$) coordination.

(c) Other significant structural variants are devoid of any coordinated solvents and include O-atom rather than N-atom donor contributions via $Fe-O-C(R)=N(Ar)$ coordination modes, as well as bridging amidato elements by means of $Fe-N(Ar)-C(R)=O-Fe$ units. The latter give rise to dimeric structures in the absence of strongly nucleophilic solvents. The simpler $[LFe(II)]^-$ case is also observed in one instance, supported by a strong N-donor ligand field.

(d) While mononuclear and dinuclear molecular entities of the type $[K(L)Fe(solv)_x]_n$ ($n = 1, 2$) have been observed, K^+ ions are also involved in intricate intermolecular links, resulting in 1-D, 2-D, and 3-D polymers. The usual K^+ contacts involve electron-rich aromatic entities and O/N-atom donor residues.

(e) Mössbauer and electrochemical data provide reference values for typical high-spin Fe(II) sites and reveal a great variety of residue-derived electronic contributions to the metal center that effect a range of Fe(II)/Fe(III) redox potentials on the order of 1.3 V.

Acknowledgment. We thank Drs. Ekk Sinn, Richard Staples, and Charles Barnes for assistance with X-ray diffraction analysis; Dr. Nathan Leigh for obtaining and interpreting mass spectra; Dr. Victoria Magrioti for obtaining the ¹⁹F NMR spectra; and Dr. Spyros Koinis for helpful discussions on the spectroscopic data. We gratefully acknowledge generous financial support (to P.S.) by the NSF (CHE-0412959) and by the NIH/NIEHS (5 P42 ES007381). We also acknowledge NSF funding (CHE-0420497) for the purchase of the diffractometer at the University of Missouri-St. Louis.

Supporting Information Available: Solid-state structures of compounds **2a**, **3a–d**, and **4** (Figures S1–S6). Summary of X-ray crystallographic data for the same compounds (Table S1). X-ray crystallographic data for all structurally characterized compounds in CIF format. Mössbauer spectra of compounds **5**, **6**, **8**, **9**, **13**, and **14** (Figures S7–S12). Cyclic voltammograms of compounds **5–15** (Figures S13–S26). The material is available free of charge via the Internet at <http://pubs.acs.org>.